Contents lists available at ScienceDirect

International Journal of Multiphase Flow

journal homepage: www.elsevier.com/locate/ijmulflow



On random walk models for simulation of particle-laden turbulent flows



Amir A. Mofakham, Goodarz Ahmadi*

Department of Mechanical and Aeronautical Engineering, Clarkson University Potsdam, NY, USA

ARTICLE INFO

Article history: Received 16 August 2019 Revised 2 November 2019 Accepted 4 November 2019 Available online 5 November 2019

Keywords

Discrete random walk model (DRW)
Continuous random walk model (CRW)
Stochastic model
Normalized Langevin equation
Deposition velocity
Concentration profiles
Particle-laden flows
Inhomogeneous turbulence flows

ABSTRACT

In this investigation, the accuracy of the discrete and continuous random walk (DRW, CRW) stochastic models for simulation of fluid (material) point particle, as well as inertial and Brownian particles, was studied. The corresponding dispersion, concentration, and deposition of suspended micro- and nanoparticles in turbulent flows were analyzed. First, the DRW model used in the ANSYS-Fluent commercial CFD code for generating instantaneous flow fluctuations in inhomogeneous turbulent flows was evaluated. For this purpose, turbulent flows in a channel were simulated using a Reynolds-averaged Navier-Stokes (RANS) approach in conjunction with the Reynolds Stress Transport turbulence model (RSTM). Then spherical particles with diameters in the range of 30 µm to 10 nm were introduced uniformly in the channel. Under the assumption of one-way coupling, ensembles of particle trajectories for different sizes were generated by solving the particle equation of motion, including the drag and Brownian forces. The DRW stochastic turbulence model of the software was used to include the effects of instantaneous velocity fluctuations on particle motion, and the steady state concentration distribution and deposition velocity of particles of various sizes were evaluated. In addition, the improved CRW model based on the normalized Langevin equation was used in an in-house Matlab code. Comparisons of the predicted results of the DRW model of ANSYS-Fluent with the available experimental data and the DNS simulation results and empirical predictions showed that this model is not able to accurately predict the flow fluctuations seen by the particles in that it leads to unreasonable concentration profiles and time-varying deposition velocities. However, the predictions of the improved CRW model were in good agreement with the experimental data and the DNS results. Possible reasons causing the discrepancies between the DRW predictions and the experimental data were discussed. The improved CRW model was also implemented through user-defined functions into the ANSYS-Fluent code, which resulted in accurate concentration distribution and deposition velocity for different size particles.

© 2019 Elsevier Ltd. All rights reserved.

1. Introduction

The availability of an accurate model for evaluation of dispersion and deposition of micro- and nano-particles in turbulent flows is of vital importance to the computer simulations of a wide range of industrial, environmental, and biomedical processes. Pneumatic conveying, ventilation systems, cloud formation, precipitation (Devenish et al., 2012; Warhaft, 2008), air pollution, sand and dust storms (Luo et al., 2016; Rahman et al., 2016; Sajjadi et al., 2016), and transport and deposition of inhaled particles in human respiratory system (Fan and Ahmadi, 2000; Cheng, 2003; Matida et al., 2004; Zamankhan et al., 2006; Longest et al., 2008; Shi et al., 2008; Longest and Vinchurkar, 2009; Tian and

E-mail address: ahmadi@clarkson.edu (G. Ahmadi).

Ahmadi, 2012; Tavakoli et al., 2012; Tian and Ahmadi, 2013; Yazdani et al., 2014; Tavakol et al., 2015; Tavakol et al., 2017) are a few examples of the processes involving particle-laden turbulent flows. Numerical simulation of these flows requires an accurate evaluation of turbulence characteristics and their interactions with particles.

The very first step for simulating turbulent flows is the selection of an appropriate method. Currently, there are three main approaches for simulating turbulent flows. The most advanced approach is the direct numerical simulation (DNS) in which all scales of turbulence down to the Kolmogorov scale are resolved. While the DNS approach is quite accurate, it is computationally expensive. The prohibitive computational cost of the DNS approach has restricted its application to large-scale industrial and environmental problems. Therefore, the applications of DNS have been limited to simple flow passages and are typically done for fundamental research studies. In the next level of accuracy is the large eddy

^{*} Corresponding author.

simulation (LES) approach that resolves the details of turbulent flows larger than the grid cell size while the subgrid-scale fluctuations are modeled (Rogallo and Moin, 1984; Lesieur et al., 2005; Sagaut, 2006). The LES requires less computational resources compared to the DNS, but still, it is computationally demanding for simulating flows in complex configurations at high Reynolds numbers of industrial and environmental interests.

The approach that is more commonly used for practical applications is the Reynolds-averaged Navier–Stokes (RANS) model. While quite economical, the RANS approach requires the use of a turbulence model and evaluates only the mean velocities and turbulence statistics. Due to the relative simplicity and computational efficiency of the RANS models, considerable attention has been given to developing appropriate turbulence models. While typically the two–equation models (e.g., k- ε , k- ω , etc.) in conjunction with the eddy viscosity assumption are used, there are also the Reynolds stress transport models (RSTM) that directly evaluate the components of Reynolds stresses and account for the anisotropy of turbulence fluctuations (Hanjalić and Launder, 1972; Durbin, 1993; Pope, 2000).

The RSTM provides the time-averaged velocity and turbulence properties; however, for certain problems such as the one involving particle dispersion and deposition, knowledge of the instantaneous turbulence fluctuations is required. In these cases, a pseudoturbulence fluctuation along the particle trajectories is generated based on the RANS evaluation of the turbulence statistical properties. Accurate evaluation of instantaneous velocity fluctuations is required for realistic evaluation of turbulent diffusion effects for accurate predictions of particle dispersion and deposition on surfaces (Loth, 2000; Bocksell and Loth, 2006). When the LES approach is used for simulating particle-laden turbulence flows, the subgrid scales (SGS) fluid fluctuating motions seen by particles should also be modeled properly for an accurate description of particle dispersion. Although the effects of SGS on particle motion were shown to be significant in several investigations (Kuerten and Vreman, 2005; Kuerten, 2005; Marchioli et al., 2008; Salmanzadeh et al., 2010; Innocenti et al., 2016), they were totally neglected in some other studies (Yeh and Lei, 1991; Uijttewaal and Oliemans, 1996; Wang and Squires, 1996; Jayaraju et al., 2008; Afkhami et al., 2015). Additional information regarding the stateof-the-art of SGS models were reported by Minier (2015), Pozorski (2017), and Marchioli (2017).

For simulating particle-laden flows, the Eulerian-Eulerian and Eulerian-Lagrangian approaches are typically used. The Eulerian-Lagrangian approach, which is more physical as it accounts for the discrete nature of particles, is used in the present study. (Taylor, 1920) was the pioneer in utilizing the Lagrangian approach, where he employed a stochastic model to simulate fluid-particle (material point) dispersion in homogeneous turbulent flows from a point source. He reported that the standard deviation of fluid-particle distances from their initial position varies linearly with time initially and then becomes proportional to the square root of time for large times. Since then, several Lagrangian stochastic models were introduced. The discrete random walk (DRW) and continuous random walk (CRW) stochastic models are widely used in CFD codes where velocities are assumed to be the summation of the mean fluid velocity and turbulence fluctuations. In the DRW and CRW models, which are not strictly derived from the Navier-Stokes equation, the velocity fluctuations are considered as Markov processes that are generated with zero mean and variances corresponding to those of turbulence velocities and appropriate time scale (Shirolkar et al., 1996; Bocksell and Loth 2001). Also, there is a Probability Density Function (PDF)-based stochastic differential equation (SDE) that is used for evaluating the fluid fluctuation velocity (Haworth and Pope 1987; Minier and Peirano 2001; Minier et al., 2004; Minier 2015; Pozorski 2017). The PDF approach was also extended for simulating the subgrid fluctuation in the LES, which is referred to as the Filter Density Function (FDF) (Givi 1989; Colucci et al., 1998; Wacławczyk et al., 2008; Innocenti et al., 2016).

In the DRW model, it is assumed that a particle interacts with an eddy for an interaction time interval t_{int} ; at the end of the interaction time interval a new random fluctuation independent of the previous one is introduced to account for the interaction time with a new turbulence eddy.

In the CRW model, a stochastic differential equation is used to find the turbulent fluctuations seen by fluid-point particles. The corresponding Langevin equation is given as

$$\frac{du_i'}{dt} = -\alpha u_i' + \lambda \xi_i,\tag{1}$$

where α and λ are coefficients, u_i' is the turbulence fluctuating velocity component and $\xi_i(t)$ is a Gaussian white noise process. The first term of the right-hand side (RHS) of Eq. (1) represents the persistence of the fluid motion that generates a correlation between successive fluctuations, and the second term includes the random variation of the fluctuations. The coefficients α and λ were evaluated by Legg and Raupach (1982) as $1/\tau_i$ and $\sigma_i \sqrt{2/\tau_i}$ where σ_i and τ_i are the RMS velocity fluctuations and the Lagrangian time scale in the i-direction.

The stochastic model proposed by Taylor and extended by others was originally established for homogenous turbulent flows. However, most practical turbulent flows, like the atmospheric boundary layer flows and flows in ducts, are inhomogeneous with spatially varying vertical root-mean-square (RMS) velocity, σ_2 , and Lagrangian time scale, τ_2 . In this regard, several researchers examined the performance of the conventional DRW and CRW models for simulating the fluctuation fields in inhomogeneous turbulent flows and proposed needed improvements for their applications (MacInnes and Bracco, 1992; Bocksell and Loth, 2001).

The studies conducted on the CRW model showed that this model could predict reasonable results for concentration profiles of fluid-particles in turbulent Atmospheric Boundary Layer (ABL) flows with an inhomogeneous vertical time scale (Hall, 1975; Reid, 1979; Wilson et al., 1981b; Legg, 1982). Wilson et al. (1981a), however, found that using the stochastic models for ABL-flows with inhomogeneous velocity fluctuations generates an unphysical inhomogeneous concentration profile. They suggested that these models lead to $c\sigma_2 = constant$ (where c is concentration), which was also reported by Thomson (1984), leading to a concentration gradient of fluid (material) point-particles in inhomogeneous flows. To rectify this defect and obtain a homogenous fluid-particle (material point) concentration in flows with variable RMS vertical velocity fluctuations, Wilson et al. (1981a) introduced a drift velocity given

$$\overline{u_2} = \tau_2 \sigma_2 \frac{\partial \sigma_2}{\partial y},\tag{2}$$

as a correction for the inhomogeneous flows.

Legg and Raupach (1982) and Ley and Thomson (1983) also noted the necessity of including a correction term to a mean pressure gradient associated with the missed Reynolds stress terms. They concluded that ignoring this correction leads to a spurious mean drift of particle trajectories. Legg and Raupach suggested using $\tau_2 \partial \sigma_2^2 / \partial y$ as the mean drift velocity and proposed a modified Langevin equation in the y-direction (perpendicular to the wall) for turbulent flows with variable vertical velocity variance. That is,

$$\frac{du'_{2}}{dt} = -\frac{u'_{2}}{\tau_{2}} + \sigma_{2}\sqrt{\frac{2}{\tau_{2}}}\xi_{2} + \frac{\partial\sigma_{2}^{2}}{\partial y}.$$
 (3)

There seems to be a factor of 2 difference between the correction mean drift velocity of Wilson et al. (1981a) and that of

Legg and Raupach (1982). Eq. (3) is referred to as a non-normalized Langevin equation (Non-normalized CRW model).

Based on the transformed coordinates used by Wilson et al. (1981a), Thomson (1984) and Durbin (1984, 1983) proposed a normalized Langevin equation given as

$$\frac{d}{dt}\left(\frac{u_2'}{\sigma_2}\right) = -\frac{u_2'}{\sigma_2\tau_2} + \sqrt{\frac{2}{\tau_2}}\xi_2 + \frac{\partial\sigma_2}{\partial y}.$$
 (4)

Later, Bocksell and Loth (2006) suggested that normalizing the Langevin equation is necessary to de-correlate the successive fluctuations generated for fluid (material) point-particles in flows with severe inhomogeneity.

More recently, Minier et al. (2014) described a more rigorous derivation of the Langevin equation based on the PDF approach of Pope (Haworth and Pope, 1987; Ahmadi and Hayday 1988; Minier, 2015; Pozorski, 2017). Minier et al. (2014) also pointed out that if it is assumed that $\tau_i = \frac{4}{3C_0}\frac{k}{\epsilon}$, where C_0 is a constant, the normalized Langevin equation for homogenous flows is identical to the Simplified Langevin Model (SLM) developed by Pope for turbulent reactive single-phase flows (Pope, 1985; Haworth and Pope, 1986). They noted that this equation does not have the exact invariance properties of inhomogeneous flows, which makes it inconsistent with the Reynolds-stress equation. Earlier, however, Iliopoulos and Hanratty (1999) and Iliopoulos et al. (2003) found a satisfactory agreement between the results obtained from Eq. (4) and the DNS results for dispersion of fluid (material) point particles and inertial solid particles in a fully developed inhomogeneous turbulent flow.

Bocksell and Loth (2006) also noted that the drift correction term for inhomogeneous flows is valid for fluid velocity fluctuations seen by fluid-particles that follow the flow. However, if the modified Langevin equation is used for generating fluid velocity fluctuations seen by inertial particles, a factor of 1/(1 + Stk), where Stk (Stokes number) is the ratio of the particle relaxation time to the local turbulent integral time scale, should be included as a coefficient for the drift correction term.

Comparisons of the results predicted by Bocksell and Loth with the DNS data for different Stokes numbers revealed that including the correction factor significantly improves the estimated concentration profiles of inertial particles. Dehbi (2008, 2010) and Jayaraju et al. (2015) examined the performance of this approach for predicting the deposition velocity and dispersion of particles in inhomogeneous turbulent flows and found reasonable agreement with the experimental data and DNS results. However, Javaraju et al. (2015) showed an overestimation of the deposition velocity of the Brownian particles in a channel flow using the Bocksell and Loth CRW model and the (ANSYS-Fluent code, 2011). They suggested that the defect of the Brownian model of the ANSYS-Fluent code (2011) was the cause of the overestimation of deposition velocity. Recently, however, Mofakham and Ahmadi (2019) compared different versions of the CRW models and showed that the CRW model based on the normalized Langevin equation, including the drift correction term of Bocksell and Loth (2006) (Normalized-CRW), predicts reasonably accurate results.

It should be pointed out that the Simplified Langevin Model (SLM) is similar to the Non-normalized-CRW model. Several recent studies showed that the SLM (the Non-normalized-CRW) overestimates the deposition velocities of micro- and nano-size particles (Mofakham and Ahmadi 2019; Chibbaro and Minier 2008; Guingo and Minier 2008; Jin et al., 2015, 2016). To improve the performance of the Simplified Langevin model, Chibbaro and Minier (2008) and Guingo and Minier (2008) had to include some ad hoc boundary conditions that they argued are in connection with the influences of the sweep and ejection events and the nearwall coherent structures. Jin et al. (2015) also tried to improve the prediction of the SLM by introducing a quadrant analysis of nor-

mal velocity fluctuations to account for the effects of the sweep and ejection events. Later, Jin et al. (2016) studied the effects of including the lift forces and the near-wall corrections of the drag and lift forces to rectify the underestimation of their earlier model for deposition velocities of small size particles but found only slight improvements.

Currently, the commercial CFD software is commonly used for extensively, including turbulent particle transport and dispersion in numerous industrial applications. In the present study, the performance of the default-DRW model of the ANSYS-Fluent 18.1 code for generating the instantaneous velocity fluctuations was carefully examined. It was found that the default-DRW model may lead to significant errors for the Reynolds-averaged Navier-Stokes (RANS) simulations of particle concentration and deposition. To improving the performance of the software, the Normalized-CRW was used. First, a fully developed turbulent airflow in a two-dimensional channel was simulated by the software using the RANS approach using the Reynolds Stress Transport model (RSTM). Then, the trajectories of a wide range of spherical particles from 10 nm to 30 µm were evaluated under the one-way coupling assumption by three approaches: (a) The discrete phase model (DPM) combined with the default random walk (DRW) stochastic model of the ANSYS-Fluent software was used. (b) The mean flow velocities, as well as root-mean-square (RMS) velocity fluctuations in different directions, were exported from the ANSYS-Fluent code and used in an in-house Matlab particle tracking code where the Normalized-CRW model was used to incorporate the effects of turbulence fluctuations on particle trajectories. (c) The Normalized-CRW model was implemented into the ANSYS-Fluent code by user-defined functions (UDFs) and the DPM model of ANSYS-Fluent was used to evaluate the particle trajectories. In each approach, a large number of particles of different sizes were tracked for long durations, and the corresponding time evolution of particle concentration profiles and deposition velocities were evaluated. The simulation results were compared with the experimental data, earlier RANS and DNS results, as well as with the empirical models. It was found that the simulation results of the in-house Matlab code and the ANSYS-Fluent software with the UDF showed that using the Normalized-CRW model for generating the fluid velocity fluctuation seen by particles markedly improved the accuracy of the model predictions for particle concentration, as well as, deposition in inhomogeneous turbulent flows.

2. Formulations

2.1. Computational Domain

In this study, it is assumed that air is flowing in a channel at room temperature (288 K) with a kinematic viscosity of v = 1.4607×10^{-5} m²/s at a Reynolds number of 3329 based on an average velocity of 5 m/s and channel half-width. The corresponding shear Reynolds number is 219 based on a wall shear velocity of $u^* = 0.32$ m/s and channel half-width. Periodic velocity boundary conditions at the inlet and outlet and the no-slip boundary condition at the upper and lower walls of the channel were imposed. The use of periodic boundary conditions makes it possible to run the flow for a long time in order to generate a fully developed flow along the channel, which eliminates the effects of developing flow near the inlet/outlet of the channel on the particle distribution. In addition, the present simulation provides sufficient time for the particles to reach their steady state distribution so that the corresponding concentration profile and deposition velocity can be evaluated. In the present simulations, the channel half-width is $H^+ = 219$, and the streamwise length of the computational domain is $L^+ = 1095$. The superscript + denotes that the parameters are normalized by the wall scaling (u^* for velocity, v/u^{*2} for time, and ν/u^* for length). There are 1000 and 100 grid points, respectively, along with the streamwise and normal direction of the channel. The grid is uniform in the streamwise direction, while it is non-uniform in the normal direction in order to provide higher resolution in the near-wall regions. To make sure that the grid is sufficiently fine and to improve the accuracy of particle trajectory estimation in the near-wall region, the first grid point is located 0.38 wall units away from the wall, which is almost one-third of the distance suggested by Tian and Ahmadi (2007). The grid becomes coarser in the core region with a growth factor of 1.08 and a maximum grid spacing of 16.5 wall units is generated at the center of the channel.

2.2. Turbulent flow field

The first step in the simulation of turbulent particle-laden flows is selecting the appropriate turbulence model. As noted before, the mean airflow field in a two-dimensional turbulent channel flow was evaluated using the RANS model of CFD software (ANSYS-Fluent version 18.1 2017), in conjunction with the Reynolds Stress transport model (RSTM). Although the RSTM model requires more computational resources compared with the conventional twoequation models (e.g., k- ε . k- ω , etc.), it has the advantage of solving directly for the components of Reynolds stresses and avoiding the need for the isotropic eddy viscosity assumption. As it was shown by Tian and Ahmadi (2007), ignoring the turbulence anisotropy degrades the accuracy of particle deposition prediction; hence, the RSTM model that captures the anisotropy of near-wall velocity fluctuations is a suitable choice. Also as it was suggested by Tian and Ahmadi (2007), in this case the enhanced wall function is used for the wall boundary condition.

Although employing the enhanced wall function improves the prediction of the RSTM model in the near-wall regions, there is another important needed correction regarding the root-mean-square (RMS) variation of normal components of turbulence fluctuations. It is well known that the RMS of normal velocity fluctuations follows a quadratic variation in the near-wall, while the streamwise and spanwise velocities vary linearly with distance from the wall. These variations are the consequence of the continuity equation (Hinze, 1975) and was verified experimentally (Finnicum and Hanratty, 1985) and also with comparison with the DNS results (Kim et al., 1987).

The ANSYS-Fluent code, however, does not predict the quadratic variation for the RMS normal fluctuations near the wall, and that leads to significant overestimation of particle deposition rate (Tian and Ahmadi, 2007). Hence, in order to provide an accurate prediction of particle deposition velocity, it is critical to account for the correct variation of normal fluctuations near the walls. Accordingly, in this study, the expression proposed by Matida et al. (2000) that was obtained by fitting the DNS data of a fully developed channel flow at $Re_{\tau} = 395$ of Antonia et al. (1991), Dreeben and Pope (1997), Moser et al. (1999) was used in order to provide the correct variation of the normal RMS velocity fluctuations in the near-wall region. That is

$$\sigma_2^+ = \frac{0.0116y^{+2}}{1 + 0.203y^+ + 0.0014y^{+2.421}}. (5)$$

Earlier, Ounis et al. (1991) and Li and Ahmadi (1993) assumed $\sigma_2^+=A\,y^{+2}$ in the near-wall region, and Tian and Ahmadi (2007) used A=0.008 for $y^+<4$.

2.3. Turbulent Fluctuations

As noted in the introduction section, the RANS-RSTM simulations predict the mean turbulent flow velocities $(\bar{u}, \bar{v}, \bar{w})$ and RMS

of velocity fluctuations. However, to include the effects of turbulent dispersion on particle distribution and deposition, the instantaneous turbulent velocity field as seen by particles during their motions must be simulated. Hence, it is necessary to utilize an accurate stochastic model to generate the local turbulence fluctuations (u', v', w') using the statistical properties evaluated from the RANS-RSTM simulation of the flow. Two stochastic turbulence models are used in this study. One is the discrete random walk (DRW) model, which is the default model of the CFD software, and the other is the Normalized-CRW. The Normalized-CRW is used in the in-house Matlab code and is also implemented in the CFD code with the use of UDFs.

2.4. Discrete random walk (DRW) model

In ANSYS-Fluent software (2017), for generating the instantaneous turbulence fluctuations, the DRW stochastic model of Gosman and Ioannides (1983) is used. The DRW model, however, is known to have spurious drift defects in inhomogeneous flows MacInnes and Bracco (1992). In this approach, the turbulence fluctuation is estimated as a discrete random walk model given as

$$u_i' = \sigma_i G_i, \tag{6}$$

where σ_i is the RMS turbulence fluctuations as obtained from the RANS simulations of the flow, and G_i s are selected from a population of independent Gaussian random numbers with zero mean and unit variance. It should be emphasized that the cross-correlation between the components of velocity fluctuations in different directions in inhomogeneous flows cannot be included by employing the standard DRW model. In this approach, it is assumed that a particle interacts with a turbulent eddy for a time interval t_{int} during which G_i is fixed. When time t_{int} is elapsed, it is assumed that the particle interacts with a new eddy and a new random number G_i is generated. The time interval is evaluated as

$$t_{int} = \min\left(\tau_e, t_{cross}\right). \tag{7}$$

In Eq. (7), τ_e is the eddy lifetime obtained from the following expression:

$$\tau_e = 2T_L, \tag{8}$$

where T_L is the Lagrangian integral time scale. When the RSTM turbulence model is used, the integral time scale can be approximated as

$$T_L \approx 0.30 \frac{k}{2}. \tag{9}$$

In Eq. (7), t_{cross} is the eddy crossing time (the time a particle needs to cross an eddy) for which the following expression was suggested by Gosman and Ioannides:

$$t_{cross} = -\tau_p \ln \left[1 - \left(\frac{L_e}{\tau_p |u - u^p|} \right) \right], \tag{10}$$

and

$$L_e = \tau_e \sqrt{\frac{2}{3}k},\tag{11}$$

where u and u^p are the fluid and particle velocity vectors. When $L_e < \tau_p | u - u^p |$, the above expression is used; otherwise, the interaction time is equal to the eddy life time. In Eq. (11), τ_p is the particle relaxation time given as

$$\tau_p = \frac{Sd_p^2 C_c}{18\nu},\tag{12}$$

where S is the density ratio, d_p is the particle diameter, and C_c is the Cunningham slip correction factor given as

$$C_c = 1 + \frac{2\lambda}{d_p} \left(1.257 + 0.4e^{-\left(\frac{1.1d_p}{2\lambda}\right)} \right),$$
 (13)

where λ is the gas mean free path.

2.5. Continuous random walk (CRW) model

As it was noted in the introduction section, based on the earlier results of Bocksell and Loth (2006) and Mofakham and Ahmadi (2019), it is expected that the Normalized-CRW model can provide accurate estimates of the instantaneous fluctuation velocities seen in inhomogeneous turbulent flows. Hence, the Normalized-CRW model, which was developed heuristically and improved over the years, is used in this study. The corresponding Langevin equation for the velocity fluctuation in the y-direction (normal to the wall) is given as

$$\frac{d}{dt}\left(\frac{u_2'}{\sigma_2}\right) = -\frac{u_2'}{\sigma_2\tau_2} + \sqrt{\frac{2}{\tau_2}}\xi_2 + \frac{1}{1 + Stk}\frac{\partial\sigma_2}{\partial y}.$$
 (14)

For the x-direction, the component of the Langevin equation is identical to Eq. (14) with the drift term neglected. Eq. (14) leads to the following Markov Chain equations for the generation of instantaneous turbulent fluctuations in the x- and y-directions (Legg and Raupach, 1982; Bocksell and Loth, 2006):

$$u_1'^{n+1} = \frac{\sigma_1^{n+1}}{\sigma_1^n} u_1'^n \exp\left(-\frac{\Delta t}{\tau_1}\right) + \sigma_1^{n+1} \left(1 - \exp\left(-2\frac{\Delta t}{\tau_1}\right)\right)^{\frac{1}{2}} G_1,$$
(15)

$$u_{2}^{\prime n+1} = \frac{\sigma_{2}^{n+1}}{\sigma_{2}^{n}} u_{2}^{\prime n} \exp\left(-\frac{\Delta t}{\tau_{2}}\right) + \sigma_{2}^{n+1} \left(1 - \exp\left(-2\frac{\Delta t}{\tau_{2}}\right)\right)^{\frac{1}{2}} G_{2} + \frac{\tau_{2}}{1 + Stk} \frac{\sigma_{2}^{n+1} \partial \sigma_{2}^{n+1}}{\partial y} \left(1 - \exp\left(-\frac{\Delta t}{\tau_{2}}\right)\right), \tag{16}$$

where $Stk = \tau_p/T_L$ and G_i are selected from a population of Gaussian random numbers with zero and unit variance at every time step.

Note that in general, a drift correction term $(\frac{1}{\sigma_1(1+Stk)}, \frac{\partial \overline{u'_1u'_2}}{\partial y})$ should also be included in Eq. (15), but since this term does not have a noticeable effect on the deposition process or concentration profiles of particles in the y-direction, it was ignored in the present study for simplicity (Iliopoulos and Hanratty, 1999). However, incorporating this term could include the possible correlation between the x- and y-velocity fluctuations and improve the consistency of this model with the Reynolds-stress equations (Minier et al., 2014).

Although the DNS investigation of Bocksell and Loth (2006) showed that the Lagrangian integral time scale is not isotropic, they reported that the estimation of Kallio and Reeks (1989) obtained from Eulerian statistics is comparable to the averaged time scales obtained from the DNS results. Hence, in the CRW model used in this study, the integral time scale is assumed to be isotropic, and the expression of Kallio and Reeks for the Lagrangian integral time scale is used for τ_1 and τ_2 . Accordingly,

$$\tau_1 = \tau_2 = T_L, \tag{17}$$

where T_L is the Lagrangian integral time scale proposed by Kallio and Reeks (1989) given as,

$$T_L^+ = T_L u^{*2} / v$$

$$= \begin{cases} 10 & \text{if } y^{+} \le 5\\ 7.122 + 0.5731y^{+} - 0.00129y^{+2} & \text{if } 5 < y^{+} < 200 \end{cases}$$
 (18)

In the present simulations, Eq. (18) for the time scale was used across the channel with half height of 219 wall units.

2.6. Particle equation of motion

In this study, in order to explore the direct effects of turbulent dispersion, the gravity and lift forces are neglected; and since the density ratio of the particle to the fluid is sufficiently large (2000), the virtual mass force that is negligibly small is also ignored. Therefore, only the drag and Brownian forces are included in the analysis. Accordingly, the corresponding equation of motion for a spherical particle is given as

$$\frac{du_i^p}{dt} = \frac{1}{\tau_p} \frac{C_D Re_p}{24} \left(u_i - u_i^p \right) + n_i(t), \tag{19}$$

where u_i^p is the ith component of particle velocity, u_i is the ith component of instantaneous fluid velocity, which is the summation of the average velocity predicted by the RANS model and the fluctuation velocity estimated by the DRW or CRW model, τ_p is the particle relaxation time defined by Eq. (12), $Re_p = d_p |u - u^p|/\nu$ is the particle Reynolds number, and C_D is the drag coefficient.

In ANSYS-Fluent code, the model proposed by Morsi and Alexander (1972) for evaluating the drag coefficient for spherical particles was used. That is,

$$C_D = a_1 + \frac{a_2}{Re_p} + \frac{a_3}{Re_p^2},\tag{20}$$

where the a_i s are constants as a function of the particle Reynolds number. In the Matlab code, the following expression is used (Hinds, 1982):

$$C_D = \begin{cases} \frac{24}{Re_p} & \text{if } \text{Re}_p \le 1, \\ \frac{24}{Re_p} \left(1 + 0.15 Re_p^{0.687} \right) & \text{otherwise} \end{cases}$$
 (21)

The Brownian force is modeled as a Gaussian white noise random process (Li and Ahmadi 1992). Accordingly, during the numerical simulation at each time step, the amplitude of the Brownian force per unit mass is given as

$$n_i(t) = G_i(t) \left(\frac{\pi S_0}{dt}\right)^{0.5},$$
 (22)

where G(t) is a zero mean, unit variance Gaussian random number and the spectral intensity of the noise, S_0 , is given by,

$$S_0 = \frac{2k_b T}{\tau_v \pi m},\tag{23}$$

where $k_b = 1.38 \times 10^{-23}$ J/K is the Boltzmann constant, T is the absolute temperature (K), and m is the mass of the particle.

A trap boundary condition is applied on the lower and upper walls for the discrete phase. That is, if a particle distance to one of the walls is less than its radius, the particle is assumed to be deposited on the wall. To keep the number of particles constant during the simulations with the CRW approach, when a particle is deposited, another particle is randomly introduced in the channel. However, due to the restriction of the ANSYS-Fluent code, it is not possible to replace the deposited particles when the default stochastic DRW model is used. For the streamwise direction, a periodic boundary condition is imposed, which means if a particle passes the outlet of the channel, it is injected with the same velocities and y-location from the inlet.

2.7. Deposition velocity and empirical models

The non-dimensional particle deposition velocity in a flow with a uniform concentration of C_0 on a wall is defined as

$$u_d^+ = \frac{J}{C_0 u^*},\tag{24}$$

where J is the particle mass flux to the wall. In a channel flow with a half-width of H^+ , the deposition velocity is estimated as

$$u_d^+ = \frac{N_d H^+}{N_0 t_d^+}. (25)$$

Here, N_0 and N_d are, respectively, the total number of particles and the number of deposited particles on the lower and upper wall

of the channel in the time interval of t_d^+ (Li and Ahmadi 1993; Nasr et al., 2009).

In order to assess the accuracy of the stochastic models for prediction of deposition velocity, the corresponding deposition velocities resulting from the models for different particle sizes are compared with the experimental data, earlier DNS simulations, and semi-empirical model predictions. The empirical equation of Wood (1981) is given as

$$u_d^+ = 0.057Sc^{-2/3} + 4.5 \times 10^{-4}\tau_p^{+2},$$
 (26)

where $Sc = \nu/D$ is the Schmidt number with D being the particle mass diffusivity given as

$$D = \frac{k_b T}{3\pi \mu d_p} C_c. \tag{27}$$

Fan and Ahmadi (1993) also developed an empirical equation based on turbulence near-wall coherent structures for predicting the deposition velocity of particles. The model of Fan and Ahmadi for a smooth surface in the absence of gravity simplifies to the following expressions:

$$u_d^+ = \begin{cases} 0.084 \ Sc^{-\frac{2}{3}} + \left[\frac{d^+}{5.23} \right]^{2/\left(1+\tau_p^{+2}L_1^+\right)} & \text{if } u_d^+ \le 0.14, \\ 0.14 & \text{otherwise,} \end{cases}$$
 (28)

where $L_1^+ = 3.08/(Sd_p^+)$.

3. Results and discussions

The flow is simulated by the ANSYS-Fluent CFD software using the RSTM model for a long time to reach a fully developed solution. It is assumed that the volume fraction of particles is sufficiently small so that the one-way coupling can be assumed. That is, the fluid carries the particles, but the effect of particles on the flow is small and can be ignored. The profiles of mean streamwise velocity, RMS streamwise and normal velocity fluctuations, turbulence kinetic energy, and turbulence dissipation rate evaluated by the RSTM model are plotted in Fig. 1 versus y^+ , which is the distance to the lower wall in wall units. For verification, these parameters for shear Reynolds number of 219 were also evaluated by the pseudo-spectral code (McLaughlin 1989; Ounis et al., 1993; Nasr et al., 2009; Mofakham et al., 2018), and the results are plotted in Fig. 1 (labeled as DNS). The DNS results of Kim et al. (1987) and Moser et al. (1999) are also shown in this figure. Fig. 1a shows a good agreement of the mean streamwise velocity obtained by the RSTM model with those of the DNS code and the DNS of Kim et al. (1987) at the shear Reynolds number of 180, as well as, with the near-wall log profile. In Fig. 1b, the RMS turbulence fluctuations in the streamwise and normal directions as predicted by the RSTM model are compared with the DNS results at the shear Reynolds number of 219 and the DNS of Kim et al. (1987) and Moser et al. (1999) at shear Reynolds number of 180. In Fig. 1c, the turbulence kinetic energy as predicted by the RSTM model is

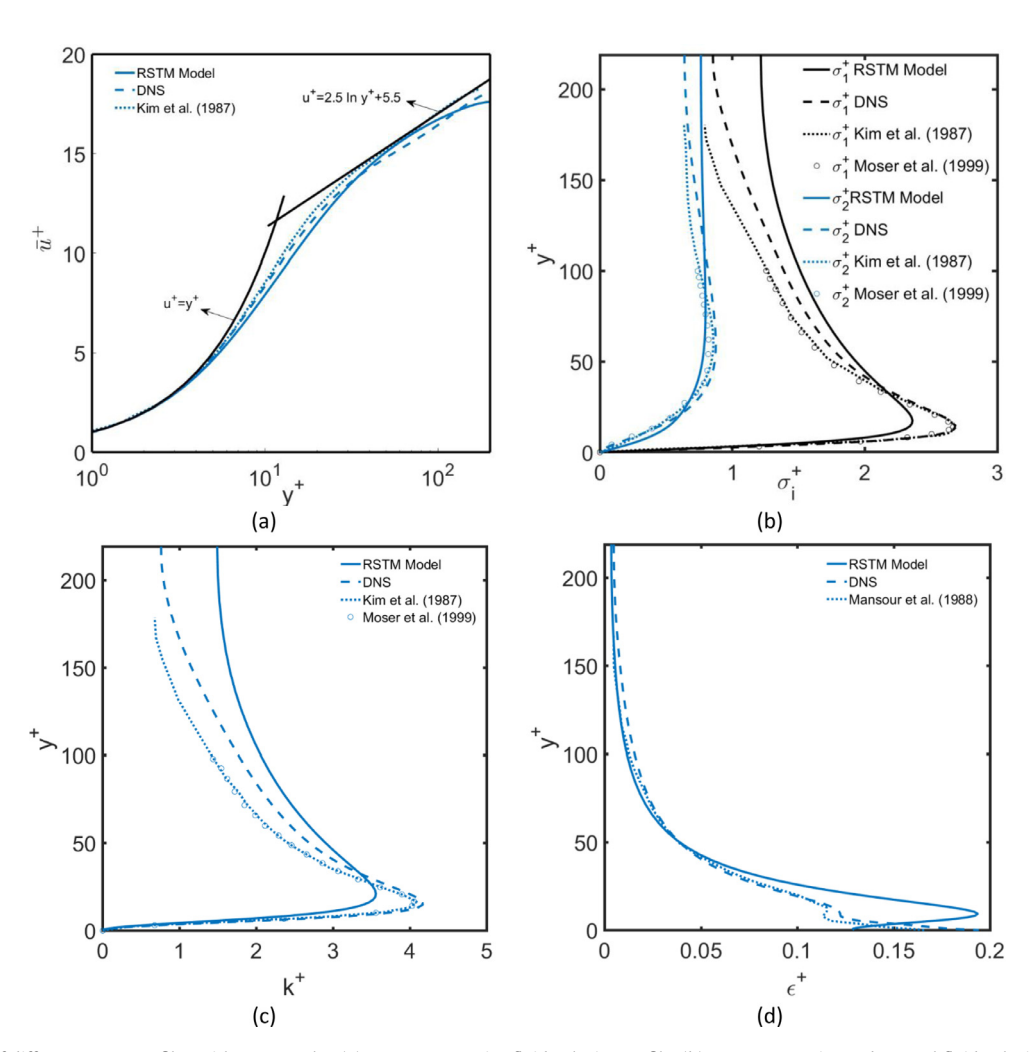


Fig. 1. Comparisons of different RANS profiles with DNS results. (a) Mean streamwise fluid velocity profile. (b) RMS streamwise and normal fluid velocity fluctuations profiles. (c) Turbulence kinetic energy. (d) Turbulence dissipation rate. $y^+ = 0$ is the lower wall and $y^+ = 219$ is the channel centerline.

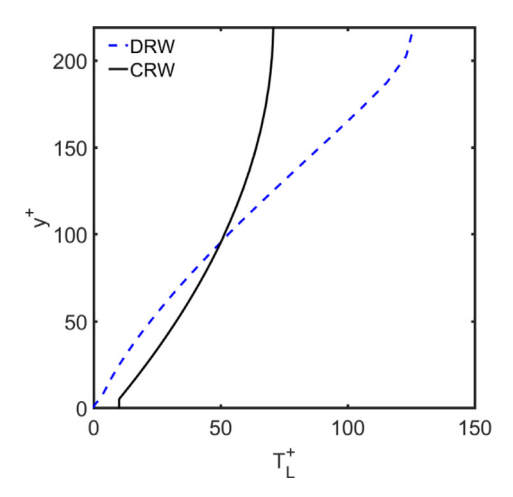


Fig. 2. The Lagrangian integral time scale profile.

compared with the DNS results at shear Reynolds number of 219 and the DNS of Kim et al. (1987) and Moser et al. (1999) at shear Reynolds number of 180. The comparisons in Figs. 1b and 1c show that the pattern of the kinetic energy predicted by the RSTM model follows the variation of the DNS data while the RSTM model underestimates the DNS results in the near-wall regions but overestimates the DNS in the core region of the channel. In Fig. 1d, the prediction of the RSTM model for the turbulence dissipation rate is compared with the DNS results at the shear Reynolds number of 219 and the DNS results reported by Mansour et al. (1988) for the shear Reynolds number of 180. The prediction of the RSTM model of the dissipation rate is in a good agreement with the DNS results, except for the near-wall regions where there are some deviations. The dissipation rate predicted by the RSTM shows a peak near the wall, while the DNS profiles show a monotonic increase toward the wall. In the region where the peak appears, the RSTM model overestimates the DNS predicted dissipation, but underestimates it at a very short distance from the wall. Despite the discrepancies between the RSTM model and the DNS prediction for the dissipation rate near the wall, the approximate agreement between the results is satisfactory.

As discussed in the formulations section, Eq. (9) is used by the ANSYS-Fluent code to evaluate the Lagrangian integral time scales for the Default-DRW model; however, for the CRW model the expression of Kallio and Reeks is going to be used for y^+ <100. Fig. 2 shows the differences between the Lagrangian integral time scales used for the DRW and CRW models.

In Fig. 3, the predicted variation of the RMS of normal fluid velocity fluctuations near the lower wall of the channel is compared with the DNS data at the shear Reynolds number of 219 and the correlation proposed by Matida et al. (2000). It is seen that the ANSYS-Fluent predictions for the velocity fluctuations normal to the wall have qualitatively different trends and are up to two orders of magnitude larger than the values obtained by the correlation of Matida et al. and the DNS data at short distances near the wall. As was noted by Tian and Ahmadi (2007), the excessively large fluctuations near the wall lead to the overestimation of the deposition velocity of particles. In this study, the prediction of ANSYS-Fluent code for σ_2 was used for the Default-DRW model, but the values of RMS velocity fluctuations are modified in the near-wall region by using Eq. (5) for the CRW model.

3.1. Particle simulations results

To assess the performance and accuracy of the stochastic models in generating instantaneous velocity fluctuations seen by parti-

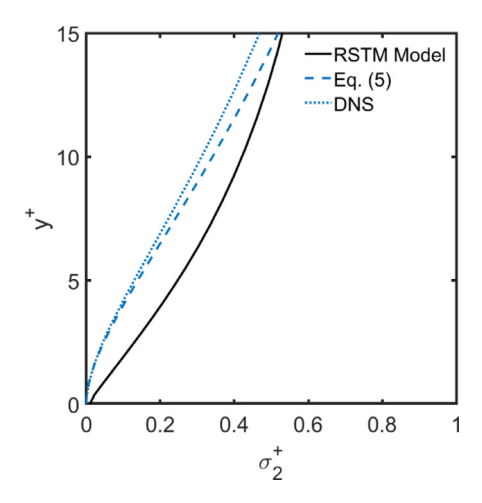


Fig. 3. Comparison of σ_2^+ near the channel lower wall as predicted by the ANSYS-Fluent code with the DNS result and the correlation proposed by Matida et al. (2000) (Eq. (5)).

cles, the resulting steady state concentration profile and deposition velocity of different size particles are evaluated for various models and the results are compared with the available experimental and DNS data in this section. In order to reduce the statistical error, 200,000 particles of a given size are injected randomly in the channel, and their subsequent motions are tracked. The initial velocities of the particles are assumed to be the same as that of the local fluid flow velocity at their initial position. While airflow velocity and RMS fluctuation are obtained by the ANSYS-Fluent code, the particle tracking and the generation of instantaneous turbulence fluctuations were done using the following two methods. (1) An in-house Matlab code was developed as post-processing to the ANSYS-Fluent code, where the Verlet integration method with a time step of 0.07 wall units was used for particle tracking, and the Normalized-CRW model was employed as the stochastic model for generating velocity fluctuations. (2) The DPM of ANSYS-Fluent code was used for tracking the particles, and both the Default-DRW model of the code and the Normalized-CRW model with the aid of UDFs were used for simulations of the velocity fluctuations. For case (2), the integration time step was picked by the ANSYS-Fluent code for each particle at every time step based on the velocity and particle relaxation time while the maximum time step was set to 0.7 wall units.

Earlier, it was shown that the random distribution of particles in a turbulence flow evolves in time and reaches a statistically stationary condition (Brooke et al., 1992; Marchioli et al., 2007). The evolution of particle distribution also affects the predicted deposition velocity. Therefore, it is necessary to track particles in turbulent flows for sufficiently long times in order to reach a quasisteady state for an accurate evaluation of particle concentration profiles and corresponding deposition velocities. In this study, particles are tracked for the duration of 10,000 wall units. In earlier studies, particle tracking was done typically for a short period of time. To assess the effect of particle size, the model predictions are obtained for a wide range of particle diameters from 10 nm to 30 µm, and the accuracy of the models for different particle sizes is evaluated. The particle diameter and the corresponding relaxation time, as well as the relaxation time in wall units for particles that are simulated in this study, are tabulated in Table 1. It should be emphasized that the integration time step used in the in-house code was 0.07 wall units, which is much smaller than the nondimensional relaxation times of particles larger than 1 µm. For smaller particle sizes (e.g., 10 nm), using a time step smaller than the particle relaxation time of 1.8×10^{-8} sec, is not practical as it makes the simulation time too long. Using a time step larger than

Table 1Particle diameters and relaxation times used in the simulations.

S = 2,000		
d_p	τ_p (s)	$ au_p^+$
30 μm 20 μm 10 μm 5 μm 3 μm 1 μm 500 nm	6.8×10^{-3} 3.0×10^{-3} 7.7×10^{-4} 2.0×10^{-4} 7.25×10^{-5} 8.9×10^{-6} 2.6×10^{-6} 2.3×10^{-7}	48.5 21.6 5.45 1.39 0.51 0.063 0.018 1.6 × 10 ⁻³
50 nm 10 nm	$\begin{array}{c} 1.0 \times 10^{-7} \\ 1.8 \times 10^{-8} \end{array}$	$7.0 \times 10^{-4} \\ 1.3 \times 10^{-4}$

the particle relaxation time essentially amounts to neglecting the particle inertia effects. Since the inertia effects of particles smaller than 1 µm is negligible, having a time step larger than the particle relaxation time does not affect the simulation results.

3.2. Fluent Default-DRW stochastic model

Using the Default-DRW model of the DPM of the ANSYS-Fluent code, the particle distribution, instantaneous velocities, and the number of deposited particles on the walls are evaluated for different sizes. Conducting ensemble averaging on the simulation results, the concentration profiles, as well as the mean velocities and

RMS velocity fluctuations of different sized particles, are evaluated and the results are reported in this section. To perform the ensemble averaging on particle concentration profiles, the bin counting method with the bin size varying according to the Chebyshev cosine function was used. Using a total number of 200 bins provided a minimum bin size of 0.027 wall units for the first bin near the wall and a maximum bin size of 3.44 wall units for the bin at the center of the channel.

In order to examine the performance of the Default-DRW model of the code, the predicted time evolutions of the normalized concentration profile of particles with different sizes are shown in Fig. 4 versus $\eta = y/H$ where y is the y-axis and H is the half height of the channel. It should be emphasized that for obtaining the normalized concentration profiles, the mean concentration in each bin is normalized by the mean concentration of the channel so that concentration 1 (shown by the dashed blue line in all concentration figures) corresponds to the uniform distribution of particles in the channel. It should be noted here that when the Default-DRW stochastic model is used, the code does not allow replacing the deposited particles to keep the total number of particles constant; therefore, the number of suspended particles in the channel and the corresponding average particle concentration decrease in time due to the deposition of particles. It should be noted that the particle concentration profiles are normalized by the updated average concentration and deposition velocities are also evaluated based on the updated average concentration; therefore, the concentration profiles and deposition velocities obtained by the Default-DRW model with variable number of particles and those of the

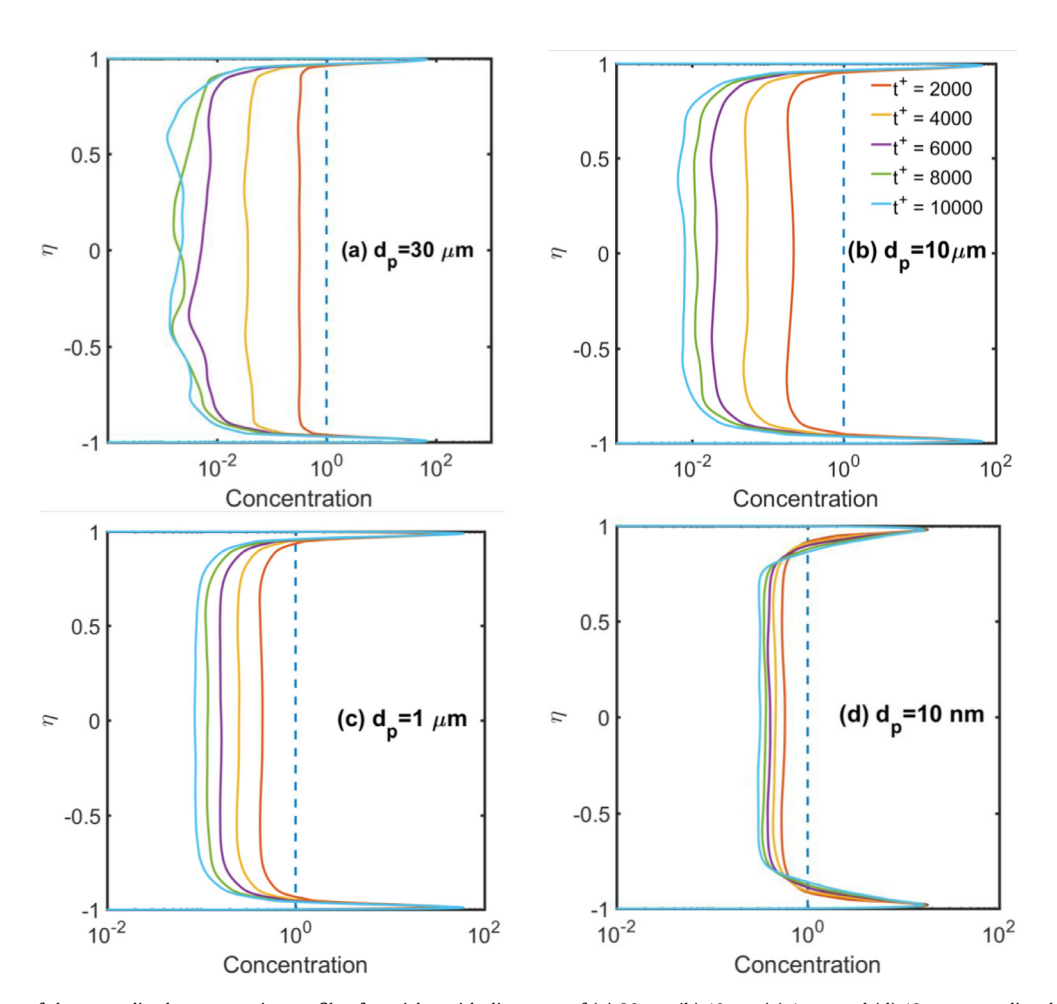


Fig. 4. Time evolutions of the normalized concentration profile of particles with diameters of (a) $30\,\mu m$, (b) $10\,\mu m$, (c) $1\,\mu m$, and (d) $10\,n m$ as predicted by the ANSYS-Fluent code using the Default-DRW model.

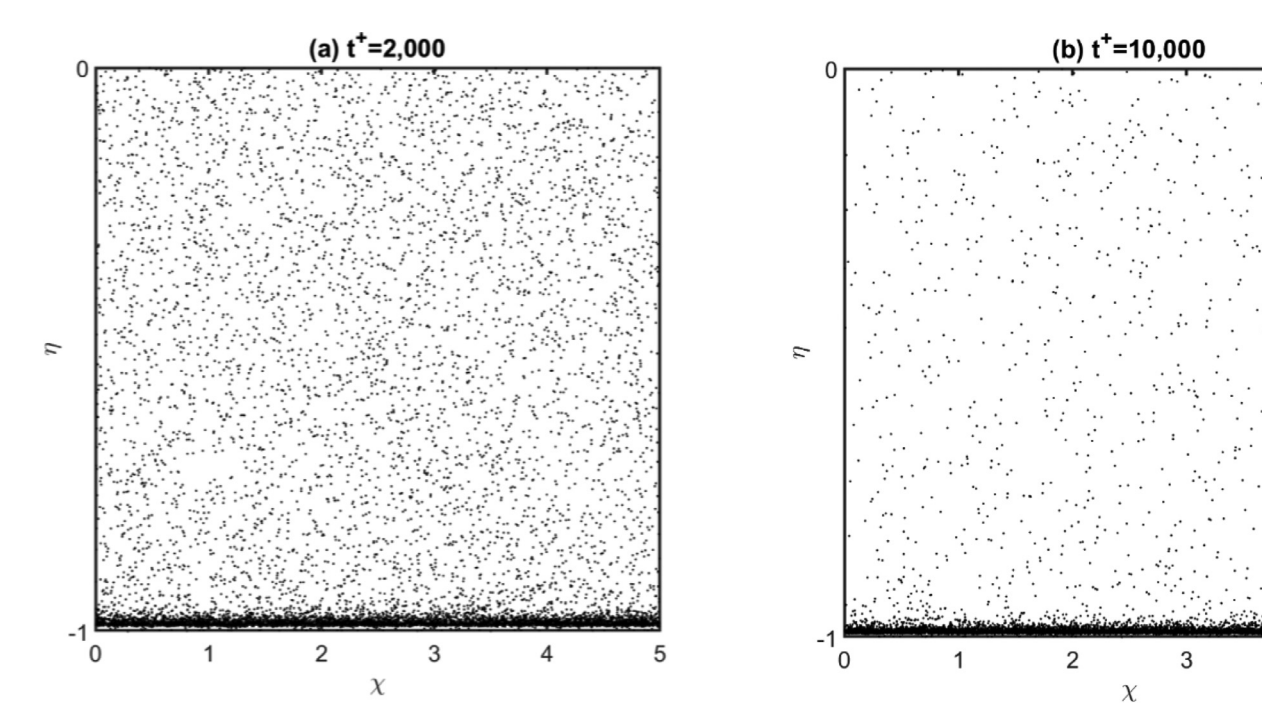


Fig. 5. The distribution of particles with a diameter of $1 \, \mu m$ at (a) $t^+ = 2,000$, (b) $t^+ = 10,000$.

Normalized-CRW with the constant number of particles are comparable.

In Fig. 4, the spatial distribution of normalized concentration of 30 µm, 10 µm, 1 µm, and 10 nm particles are shown. This figure shows that the Default-DRW model predicts an accumulation of particles of all sizes in the near-wall regions. It was observed experimentally (Rashidi et al., 1990; Kaftori et al., 1995) and numerically by the DNS approach (McLaughlin 1989; van Haarlem et al. 1998; Marchioli and Soldati 2002; Narayanan et al., 2003; Nasr et al., 2009) that particles with the dimensionless relaxation time larger than 3 tend to migrate from regions with relatively high turbulence intensity to regions with low turbulence intensity, which results in accumulation of particles in the near-wall regions. This effect is referred to as the turbophoresis phenomenon (Caporaloni et al., 1975; Reeks 1983; Reeks 1981; Young and Leeming 1997). Therefore, having a high concentration of large particles in the near-wall regions is expected. However, submicron particles with $\tau_p^+ \ll 1$ are expected to behave like fluid-tracer particles; therefore, the spatial variation of turbulence intensities should not affect the distribution of small particles, and their concentration should stay roughly uniform. Fig. 4 shows that the ANSYS-Fluent code does not predict the correct uniform concentration profile even for the 10 nm particles with $\tau_p^+=1.3\times 10^{-4}$ for which the Brownian effect is significant, and the distribution of particles should stay uniform except at the short distances near the wall where the concentration approaches zero at the wall.

Fig. 5 clearly illustrates the predicted abnormal distribution of particles with a diameter of 1 μ m after 2000 and 10,000 wall units by the ANSYS-Fluent code using the Default-DRW model. In this figure, $\chi = x/H$, where x is the x-axis, and H is the half height of the channel. For 1 μ m diameter with $\tau_p^+ = 6.3 \times 10^{-2}$, it is expected that these particles would follow the turbulent eddies and particle migration and preferential concentration should not be observed. In addition, for this size, the Brownian effects are small, resulting in very low deposition on the walls. Hence, it is expected that the 1 μ m particles have a uniform distribution across the duct with a small deposition velocity. The present simulations show that only 20 particles out of 200,000 initial particles are deposited

in 10,000 wall units; therefore, the predicted deposition velocity is very small. Fig. 5a, however, shows that the particles accumulate in the near-wall regions, and Fig. 5b shows that the core of the channel is depleted of particles, and most particles migrate to the near-wall regions after 10,000 wall units.

In order to further explore the DRW stochastic model in generating the turbulence fluctuations, the predicted mean streamwise and normal velocities, as well as the root-mean-square (RMS) streamwise and normal velocity fluctuations of particles of different sizes are compared with the corresponding values of the fluid point particle in Fig. 6.

Fig. 6a shows that at the center of the channel, the mean streamwise velocity of particles is slightly smaller than that of the fluid. However, in the near-wall regions up to about 100 wall units, the mean streamwise velocity of particles of different sizes matches with that of the fluid flow except for particles with a diameter of 30 μ m whose mean streamwise velocity is slightly higher. The larger mean streamwise velocity of 30 μ m in the near-wall regions is due to the high rate of particle migration from the core of the channel with relatively higher velocities to the near-wall regions and the large relaxation time of 30 μ m particles that allows the particles to keep their velocities. Hence, the mean streamwise velocity of 30 μ m particles is somewhat higher in the near-wall regions.

Fig. 6b shows that the mean normal velocity of particles maintains a small migration velocity toward the wall. The positive and negative normal values, respectively, in the upper and lower region of the channel, are expected due to the net migrations of particles from the core region toward the walls. It is well known that the effect of the turbophoresis gets weaker as particle size decreases, which is consistent with the findings of Fig. 6b that the magnitude of the mean normal velocity of particles gradually decreases as particle size decreases from $30\,\mu m$ to $1\,\mu m$.

The predicted RMS of particle streamwise velocities for different size particles are shown in Fig. 6c. This figure shows that the RMS of streamwise velocity fluctuations of large size particles (30 µm) is smaller than the RMS of streamwise fluid velocity fluctuations in the core of the channel. This is because of the large

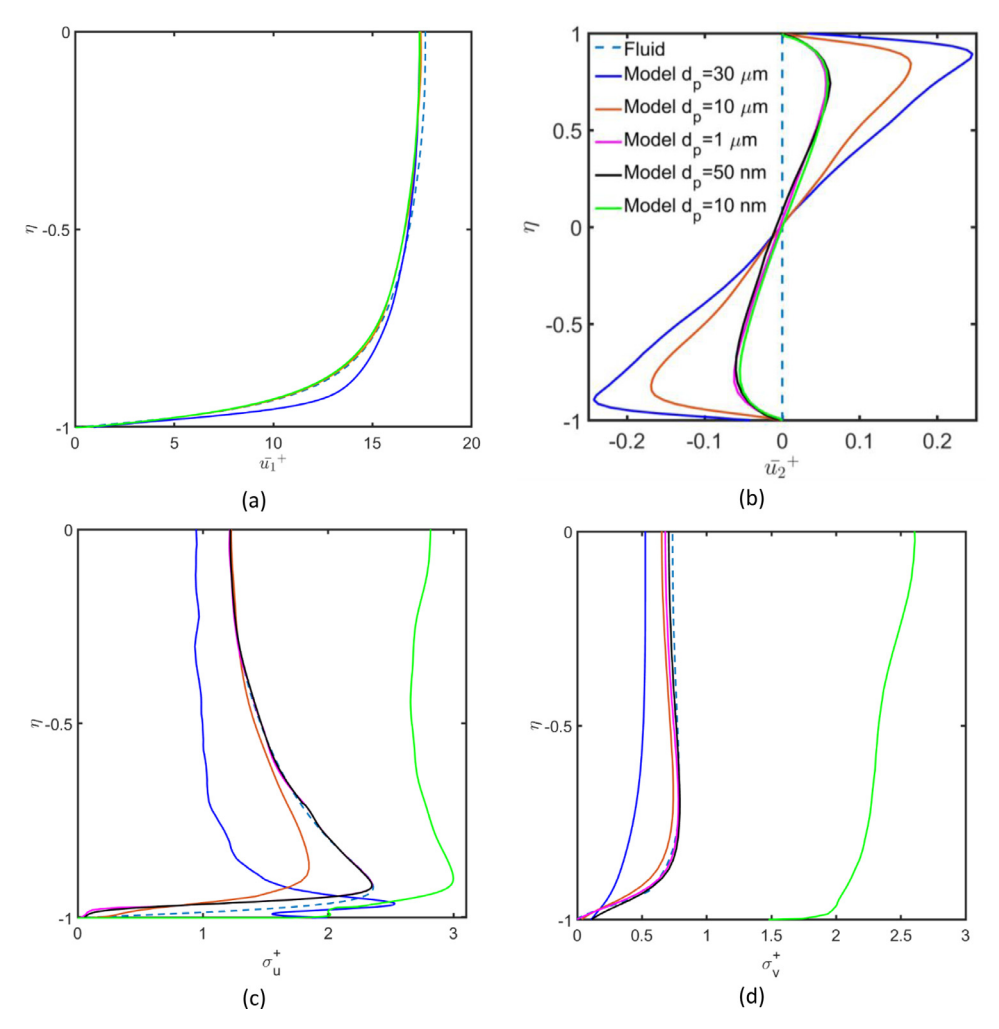


Fig. 6. Comparison of the predictions of the Default-DRW stochastic model of ANSYS-Fluent for (a) mean streamwise velocity, (b) mean normal velocity, (c) RMS streamwise velocity fluctuations, and (d) RMS normal velocity fluctuations of particles with diameters of $30\,\mu m$, $10\,\mu m$, $10\,\mu m$, and $10\,n m$ with the corresponding fluid mean velocity and RMS profiles.

particle relaxation time that filters out the high frequencies of fluid fluctuations. Although the RMS streamwise velocity fluctuations of particles are smaller than that of the fluid in the core of the channel, they are higher in the near-wall region, which is again due to the rapid migration of 30 µm particles from the core region toward the near-wall regions. With higher streamwise velocity, the mean and RMS streamwise velocities of large particles in the near-wall regions become larger than that of the fluid flow. As particle size decreases to around 1 µm, their relaxation time becomes small and their RMS streamwise velocity fluctuations become similar to that of the fluid. The RMS streamwise velocity fluctuations of 50 nm particles is almost the same as that of 1 um particles; however, with further decrease of particle size to 10 nm, the RMS streamwise velocity fluctuations dramatically increases due to the significant effects of the Brownian excitation. It is worth mentioning that the turbulence-induced RMS velocity of the 10 nm particles is comparable to that of the fluid. The difference between the RMS of 10 nm particle velocity fluctuations with that of fluid is due to the Brownian forces given by Eq. (22) which is proportional to $1/\Delta t$. That is, the RMS of particle velocity fluctuations is inversely proportional to the square root of the time step picked for particle tracking by the code. Hence, if a smaller time step is picked, a larger RMS velocity is predicted, while the particle diffusivity, which is proportional to $\sigma_i^2 \Delta t$, is fixed.

Fig. 6d compares the predicted RMS of particle normal fluctuation velocity with that of the fluid flow. It is seen that the RMS normal velocity of 30 µm is smaller than that of the fluid, and similar to Fig. 6c with the decreasing size of particles the RMS of particles normal velocity fluctuations get closer to that of the fluid. The RMS of normal velocity fluctuations of submicron particles larger than and equal to 50 nm is similar to that of the fluid. For 10 nm particles, the Brownian excitation dramatically increases the normal velocity fluctuations, and the corresponding total RMS velocities become much larger than that of the fluid.

As shown in Fig. 4, the Default-DRW model predicts an evolving concentration profile for all particle sizes implying that particles are continuously migrating from the core region to the nearwall regions with time. To further clarify the trend of variations of particle parameters in the near-wall region, the profiles of particle concentration and the RMS streamwise and normal velocity fluctuation of different size particles are plotted in Fig. 7. Fig. 7a shows that at distances less than 15 wall units from the wall, the RMS streamwise velocity fluctuations of $10\,\mu\text{m}$, $1\,\mu\text{m}$, and $50\,\text{nm}$ particles are much smaller than that of the fluid. In contrast, the $30\,\mu\text{m}$ and $10\,\text{nm}$ particles have larger RMS streamwise velocity fluctuation values in the near-wall region compared to that of the fluid flow. While the RMS streamwise velocity fluctuations of $30\,\mu\text{m}$ are higher than that of the fluid, the corresponding RMS velocity reduces somewhat toward the wall and then increases to a non-zero

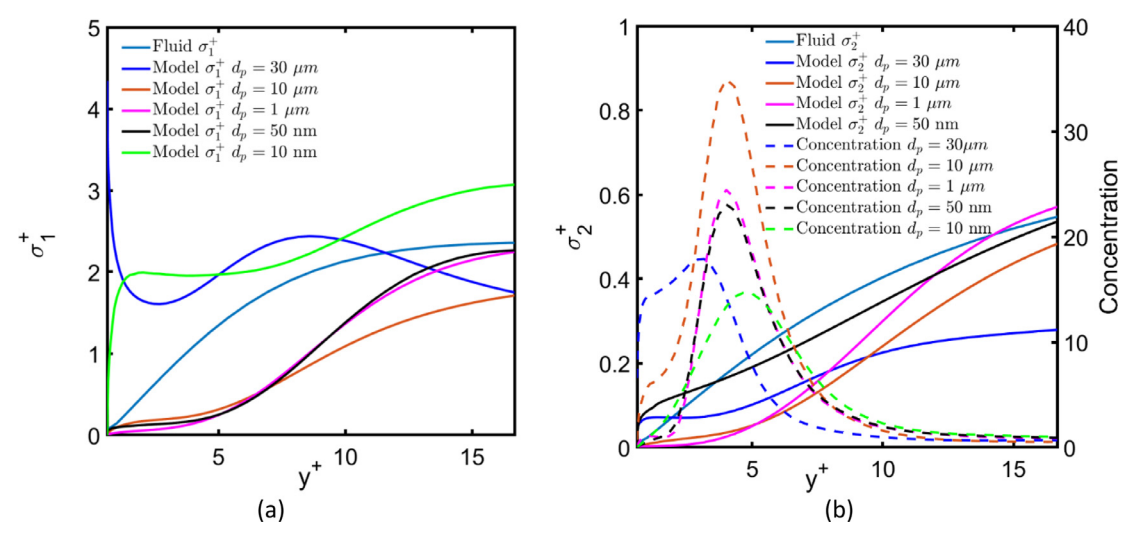


Fig. 7. Comparisons of the (a) RMS streamwise fluctuation velocity profiles and (b) RMS normal fluctuation velocities and concentration profiles of particles with diameters of 30 µm, 10 µm, 1 µm, 50 nm, and 10 nm near the lower wall of the channel as predicted by the Default-DRW stochastic model of the ANSYS-Fluent code.

value at the wall. As seen in Fig. 7a, similar to $30\,\mu m$ particles, while the RMS streamwise velocity fluctuations of $10\,n m$ particles are larger than that of the fluid, they are also damped out sharply at the distances of a few wall units from the wall and drop to zero at the wall. Thus, Fig. 7a shows that the RMS streamwise velocity fluctuations of different size particles are damped in a band near the wall, and they do not follow the variation pattern of the fluid RMS streamwise velocity fluctuations.

Fig. 7b also shows that the RMS normal velocity fluctuations of different size particles are damped in the near-wall regions with $y^+ < 8$, even if they maintain large normal velocity fluctuations away from the wall or at very short distances $(y^+ < 2)$ as a result of the Brownian effects (50 nm particles) or the inertial effects (30 μ m particles). For better comparisons, the RMS normal velocity fluctuations of 10 nm, which are much larger than those of other particle sizes and fluid, are not plotted in this figure.

The concentration profiles of different size particles are also plotted in Fig. 7b. Fig. 7b shows an unrealistically high concentration of particles in the near-wall region in the range of $2 < y^+ < 8$ for all particle sizes where the intensity of their normal fluctuation velocity is markedly underestimated.

It is expected that the RMS velocity fluctuations of 1 μ m particles would be very close to that of fluid velocity fluctuations. However, Fig. 7 indicates that the evaluated RMS velocity fluctuations of 1 μ m particles in the near-wall regions are much smaller than those of the fluid. Therefore, it is concluded that the Default-DRW model underestimates the fluid turbulence fluctuations in both streamwise and normal directions in the near-wall regions. The reduction of the normal turbulence fluctuations in the near-wall regions leads to trapping of particles in the $2 < y^+ < 8$ region in that they do not experience sufficiently large fluctuations to allow their deposition on the walls or a return to the core region, leading to the high concentration in this zone.

From the results obtained by the Default-DRW stochastic model of the ANSYS-Fluent code, the normalized number of particle deposition with diameters of 30 μ m to 10 nm are plotted versus time (t^+) in Fig. 8a. Using Eq. (25), the corresponding deposition velocities are also evaluated and plotted in Fig. 8b. These figures clearly show that the rate of deposition and the predicted deposition velocities computed from the Default-DRW stochastic model are not stationary but evolving with time.

Fig. 8b shows that the predicted deposition velocity of $30\,\mu m$ to $1\,\mu m$ (inertial) particles is relatively high at the beginning of

simulations when the distribution of particles across the channel is uniform; however, the deposition velocity decreases significantly in time and tends to zero after 5000 wall units. Since the total concentration of particles reduces in time as a result of particle deposition on the walls, one may conclude that the decrease of deposition velocities is due to the reduction of the total number of particles; however, for 10 µm particles for which less than 10% of the total number of particles are deposited after 10,000 wall units, the predicted deposition velocity still approaches a very small value. It should also be emphasized that for the calculation of deposition velocities, the updated average concentrations are used. Hence, the reduction of particle concentration is not the main reason for the decrease of deposition velocity toward zero. As noted in the discussion of Fig. 7, implementing the Default-DRW model leads to the accumulation of particles in the near-wall regions where the model significantly underestimates the velocity fluctuations seen by particles. Therefore, since the turbulence inertia impaction is the only mechanism responsible for the inertial particle deposition, as particles accumulate in the near-wall regions with low fluctuation velocities, they cannot deposit, which leads to the reduction of the deposition velocity with time.

The variation of the predicted deposition velocity of submicron particles in time is shown in Fig. 8b. The trend of variation of the deposition velocity of 500 nm particles is similar to that of the inertial particles. However, by decreasing the size of particles and increasing the Brownian effects, the trend is gradually changed. The predicted deposition velocities of 100 nm or 50 nm particles show a rapid increase for a very short time, followed by a slight reduction, but then an increase at larger times. For the smallest sizes of 50 nm and 10 nm, the deposition velocities increase and roughly converge to certain stationary values. The trend of velocity deposition of ultra-fine particles differs from that of the inertial particles because the submicron particles are transported into the viscous sublayer by turbulent diffusion but are deposited on the wall by the Brownian diffusion. Therefore, since the intensity of the Brownian force is inversely proportional to the particle diameter, the chance for deposition increases as the particle becomes smaller.

The results presented in Figs. 4–8 show that the Default-DRW stochastic model of ANSYS-Fluent code (version 18.1) does not perform well for predicting particle concentration profiles and stationary deposition velocities. MacInnes and Bracco (1992) and Bocksell and Loth (2001) suggested the need to include the drift correction term in the DRW model to prevent the non-physical high

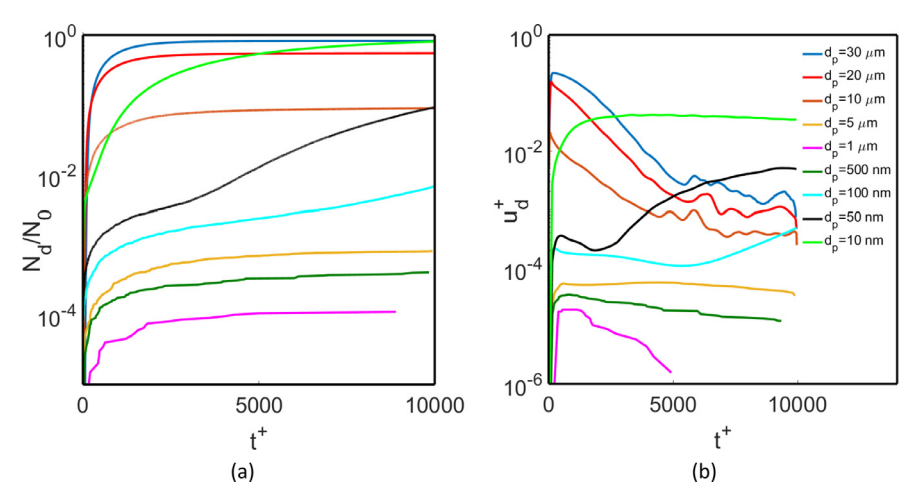


Fig. 8. (a) The normalized number of deposited 30 µm to 10 nm particles versus time. (b) The predicted deposition velocity for 30 µm to 10 nm particles.

concentration of particles in inhomogeneous turbulent flows. Accordingly, as mentioned in the ANSYS-Fluent theory guide (2017), the DRW model in which the correction term has been ignored is not able to predict a homogeneous concentration profile for small particles. The results presented here show that underestimating the velocity fluctuations seen by particles adjacent to the walls increases the gradient of velocity fluctuations in these regions, which amplifies the adverse effects of the absence of the drift correction term. Thus, it is not possible to predict a realistic, steady concentration profile and deposition velocity with the use of the Default-DRW model for particles in the range of $10\,\mathrm{nm}$ to $30\,\mathrm{\mu m}$.

3.3. Matlab Normalized-CRW stochastic model

To improve the accuracy of the ANSYS-FLUENT software for evaluation of particle dispersion and deposition, it is necessary to improve the turbulence stochastic model. However, since it is not possible to directly modify the Default-DRW stochastic model of the software, the Normalized-CRW model is incorporated into the code with the use of UDFs. Prior to implementing this model into the software, the concentration and deposition rates of particles are estimated using an in-house particle tracking Matlab code in which the Normalized-CRW stochastic model is used. The advantage of using the in-house code is that the details of the tracking method, the DPM boundary conditions, the Brownian and the drag force models, as well as the random number generator function. are known. Hence, the other possible unknowns do not affect the results. In addition, by comparing the predicted results from the in-house code and the ANSYS-Fluent code using the same stochastic model, the accuracy of the approach could be verified.

The mean velocity and RMS fluid velocity fluctuations in the streamwise and normal directions are exported from the ANSYS-Fluent channel flow simulation and used in an in-house particle tracking Matlab code. The particle sizes tabulated in Table 1 are tracked for 10,000 wall units using the Normalized-CRW model to produce the instantaneous fluid fluctuations seen by particles. Ensemble averaging is used and the normalized concentration profiles, the mean velocity, and the RMS velocity fluctuations profiles, as well as the deposition velocity of various particle sizes, are evaluated, and the results are described in this section.

To understand the performance of the code in evaluating particle concentration, the evolution of the normalized concentration profile in time and the steady normalized concentration of different size particles are, respectively, shown in Figs. 9 and 10. For finding the normalized concentration profiles, the same procedure described in Section 3.2 on ANSYS-Fluent Default-DRW stochastic

model is used. Here, however, the deposited particles are replaced in the channel randomly so that the total number of particles is kept constant during the simulations.

Fig. 9 shows that the concentration profile at times of 2000 and 10,000 wall units are similar, confirming that the steady state profile is reached after 2000 wall units. This is in contrast with the particle concentration profiles predicted by the Default-DRW stochastic model of ANSYS-Fluent code shown in Fig. 4, where the concentration in the near-wall regions is continuously increasing with time while the channel core region is being depleted. In fact, for every particle size, a steady concentration is predicted by the in-house Matlab code. Here only the time evolution of the normalized concentration profiles for three particle sizes of $30\,\mu\text{m}$, $1\,\mu\text{m}$, and $10\,\text{nm}$ belonging to three different regimes of deposition are reported for brevity.

To further elucidate the performance of the in-house Matlab code in predicting the steady concentration in the channel, the normalized concentration profiles of large size particles and submicron particles after 10,000 wall units are, respectively, shown in Figs. 10 and 11.

Fig. 10a shows the effects of the turbophoresis on particles with diameters larger than 1 µm that results in the migration of particles from the core region to the near-wall region, leading to a high particle concentration near the wall and a concentration less than 1 in the core of the channel. For exploring the variations in the near-wall region, the concentration profiles near the lower wall are plotted in Fig. 10b. It is seen that the concentration peak is highest for 10 and 20 µm particles. As particle diameter (relaxation time) increases, the particle retains its velocity for a longer time, which results in the enhancement of turbophoresis effects (van Haarlem et al. 1998; Rashidi et al., 1990; Brooke et al., 1994; Young and Leeming 1997). The concentration of particles in the near-wall region is affected by both the turbophoresis effects and the deposition velocity of particles, which explains why the peak of normalized particle concentration in the near-wall region does not monotonically increase with size. Fig. 10b shows that the peak of particle concentration increases from around 2.5 for 5 µm to 40 for 10 µm due to the increase of the turbophoresis effects, but it decreases to about 37 for 20 µm and then drops to 7 for 30 µm particles as a result of the increase in the particle deposition velocity.

Fig. 11 shows the concentration profiles of submicron particles. As it is seen in Fig. 11, the concentration stays uniform around 1 for different submicron particles, and it gradually decreases in a thin boundary layer to zero at the wall.

In Fig. 12, the prediction of the in-house Matlab code for the mean and RMS particle velocities in the streamwise and normal

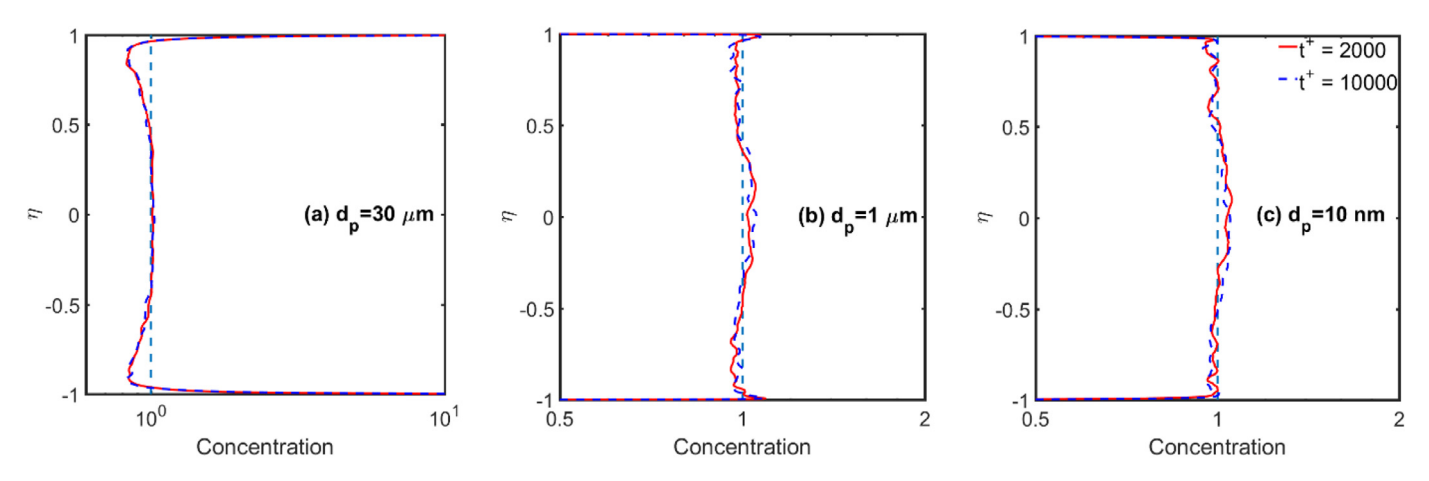


Fig. 9. Time evolutions of the normalized concentration profiles of particles with diameters of (a) $30\,\mu m$, (b) $1\,\mu m$, and (c) $10\,n m$ as predicted by the in-house Matlab code using the Normalized-CRW stochastic model.

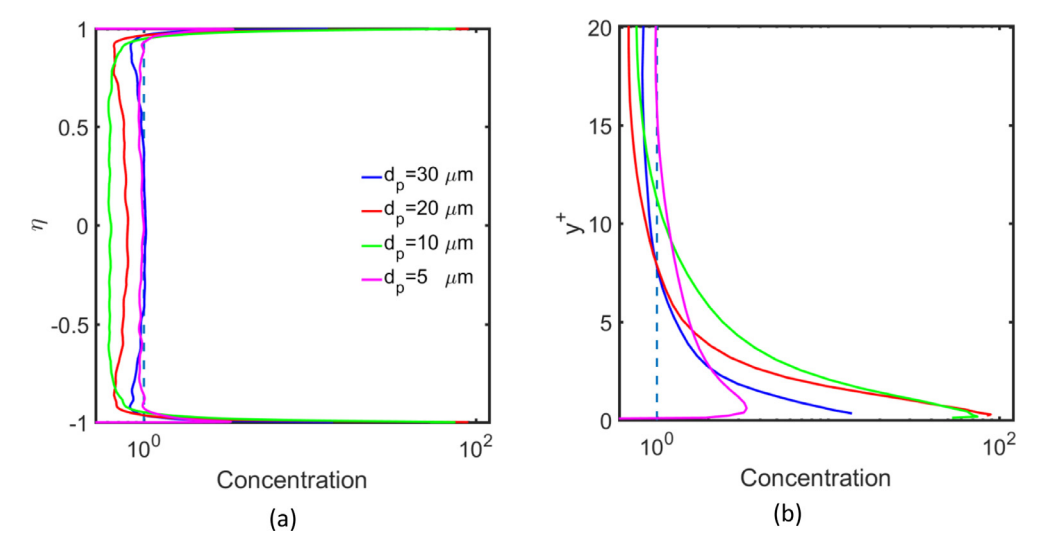


Fig. 10. Concentration profiles obtained by the in-house Matlab code using the Normalized-CRW stochastic model for particles with diameters of 30 μm to 5 μm plotted (a) along the channel and (b) near the lower wall.

directions are compared with the corresponding fluid profiles. Fig. 12a shows that the mean streamwise velocity profiles of different size particles match with that of the fluid, except for the large size $30\,\mu m$ particles that have slightly larger velocities in the near-wall regions.

Fig. 11 shows that, in contrast to the Default-DRW model, the Normalized-CRW model does not predict a migration of submicron particles to the near-wall regions; therefore, the mean normal velocity of submicron particles plotted in Fig. 12b are much smaller (nearly zero) than the corresponding profiles resulting from the DRW model shown in Fig. 6b. For large size particles, Fig. 10 confirms the formation of high particle concentration in the nearwall regions and migration of particles from the core region to the near-wall regions, which is consistent with a net mean velocity toward the walls shown in Fig. 12b. Fig. 12b also shows that for larger particles, there is a larger mean normal velocity due to the stronger turbophoresis effects. Since the high concentration values predicted for the large size particles resulting from the Normalized-CRW model shown in Fig. 10 are considerably smaller than the high concentration predicted by the Default-DRW model shown in Fig. 7b, the mean normal velocity profile evaluated for large size particles in Fig. 12b are smaller than the corresponding velocity profiles plotted in Fig. 6b.

The streamwise and normal RMS particle velocity fluctuations are shown, respectively, in Figs. 12c and 12d. Due to the large relaxation time of 30 µm particles, the corresponding streamwise and normal RMS velocity fluctuations are generally smaller than those of the fluid except for the streamwise RMS velocity fluctuations in the near-wall regions. The higher streamwise RMS velocity fluctuations of 30 µm particles in the near-wall regions is again attributed to the migration of particles from the core region, with higher streamwise velocity fluctuations to the near-wall regions. Due to the lower relaxation time of the 20-10 µm particles, the corresponding RMS velocity fluctuations of 20-10 µm are more similar to those of the fluid compared to the 30 µm particles. By decreasing the size of particles to less than 10 µm, down to 50 nm, the evaluated RMS velocity fluctuations of particles become very similar to those of fluid flow. For 10 nm particles, however, the evaluated RMS velocity fluctuations are higher than those of the fluid due to the effects of the Brownian motions. As was noted in the discussion of Fig. 6, the difference between the evaluated RMS velocity fluctuations of the particles and those of the fluid is proportional to the magnitude of the Brownian excitation forces that are a function of $1/\sqrt{\Delta t}$. Since the dynamic time steps picked by the ANSYS-Fluent code for submicron particles are generally smaller than the fixed time step of 0.07 wall units used for

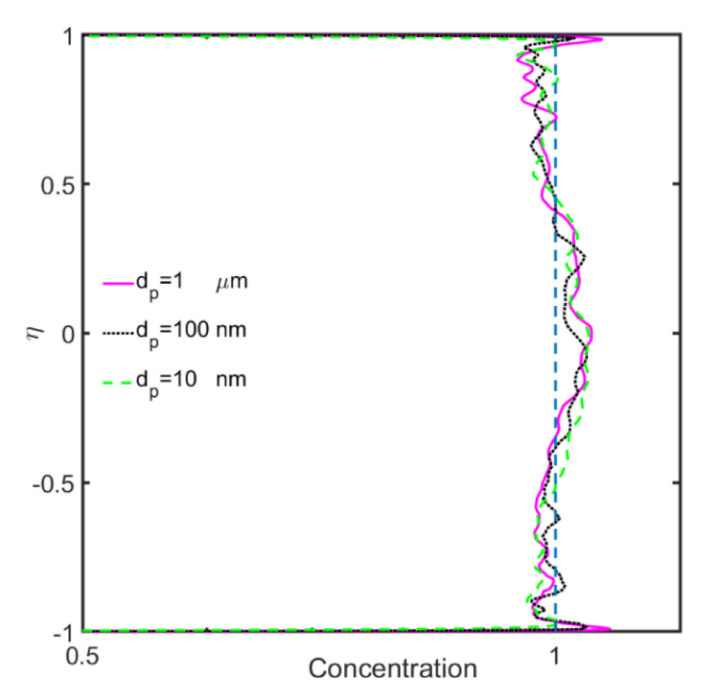


Fig. 11. Concentration profiles obtained by the in-house Matlab code using Normalized-CRW stochastic model for particles with diameters of $1\,\mu m$, $50\,n m$, and $10\,n m$.

the simulations conducted by the in-house Matlab code, the difference in Fig. 12 is not as large as that seen in Fig. 6.

It should be emphasized that the agreement between the mean velocity and the RMS velocity fluctuation profiles of small-inertia (1 μ m) particles with the Eulerian (fluid) predictions confirms that the Normalized-CRW model is consistent with the Eulerian formulations. Additional discussion of the consistency of the hybrid Eulerian/Lagrangian approach was reported by Chibbaro and Minier (2011).

As shown in Figs. 6 and 7, the RMS particle velocity profiles resulting from the Default-DRW model are smaller than those of the fluid in the near-wall regions. Figs. 12c and 12d, however, show that except for 30 µm particles, which maintain a larger RMS velocity relative to the fluid, the RMS velocity profiles of the other sizes follow the RMS velocity profiles of the fluid, and they are not damped in the near-wall regions. A more detailed comparison between the RMS particle velocity fluctuations resulting from the Normalized-CRW model and those of the Default-DRW model is made in Section 3.5.

3.4. Fluent Normalized-CRW stochastic model

Since accurate results were obtained by the in-house Matlab code using the Normalized-CRW stochastic model, this model was implemented into the ANSYS-Fluent software using UDFs. Implementing the Normalized-CRW model instead of the Default-DRW

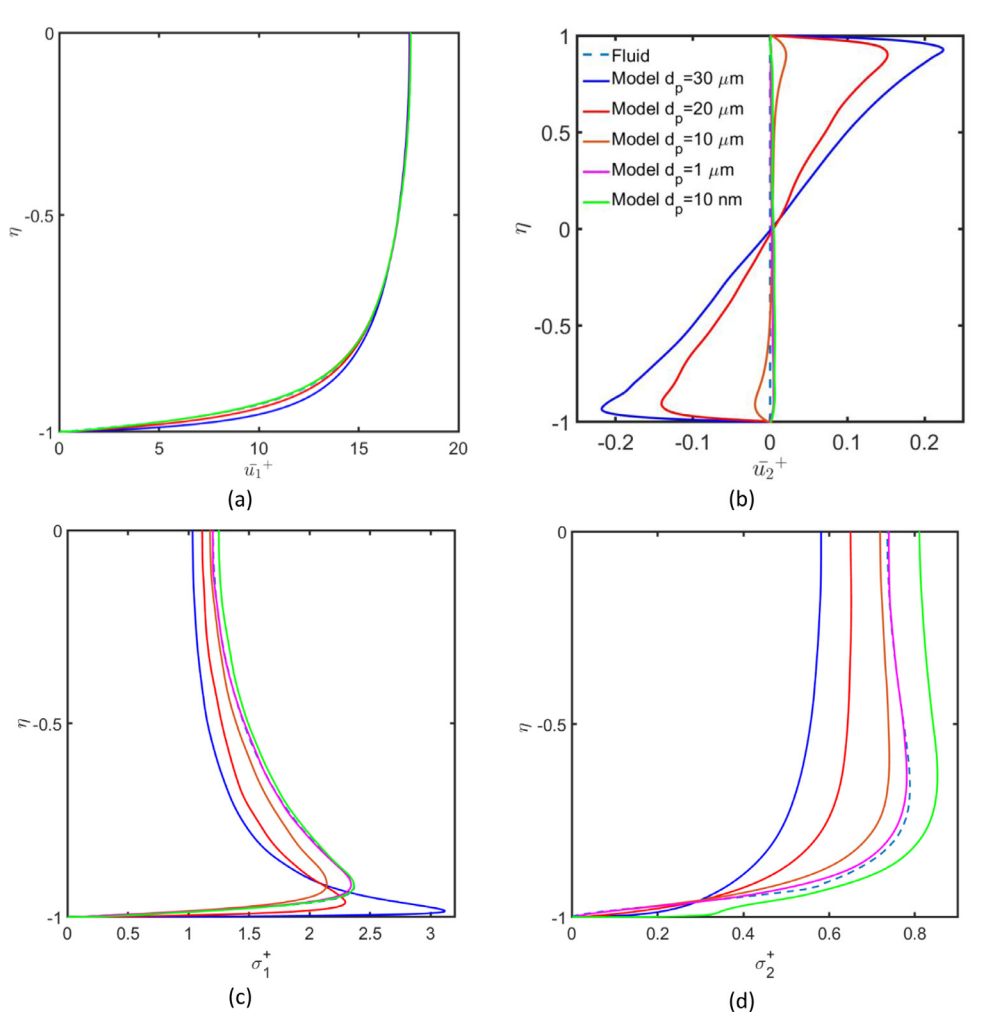


Fig. 12. Comparison of (a) mean streamwise velocity, (b) mean normal velocity, (c) RMS streamwise velocity fluctuations, and (d) RMS normal velocity fluctuation profiles of particles with diameters of $30\,\mu m$, $10\,\mu m$, $1\,\mu m$, $50\,n m$, and $10\,n m$ as predicted by the in-house Matlab code using the Normalized-CRW model with the corresponding fluid velocity profiles.

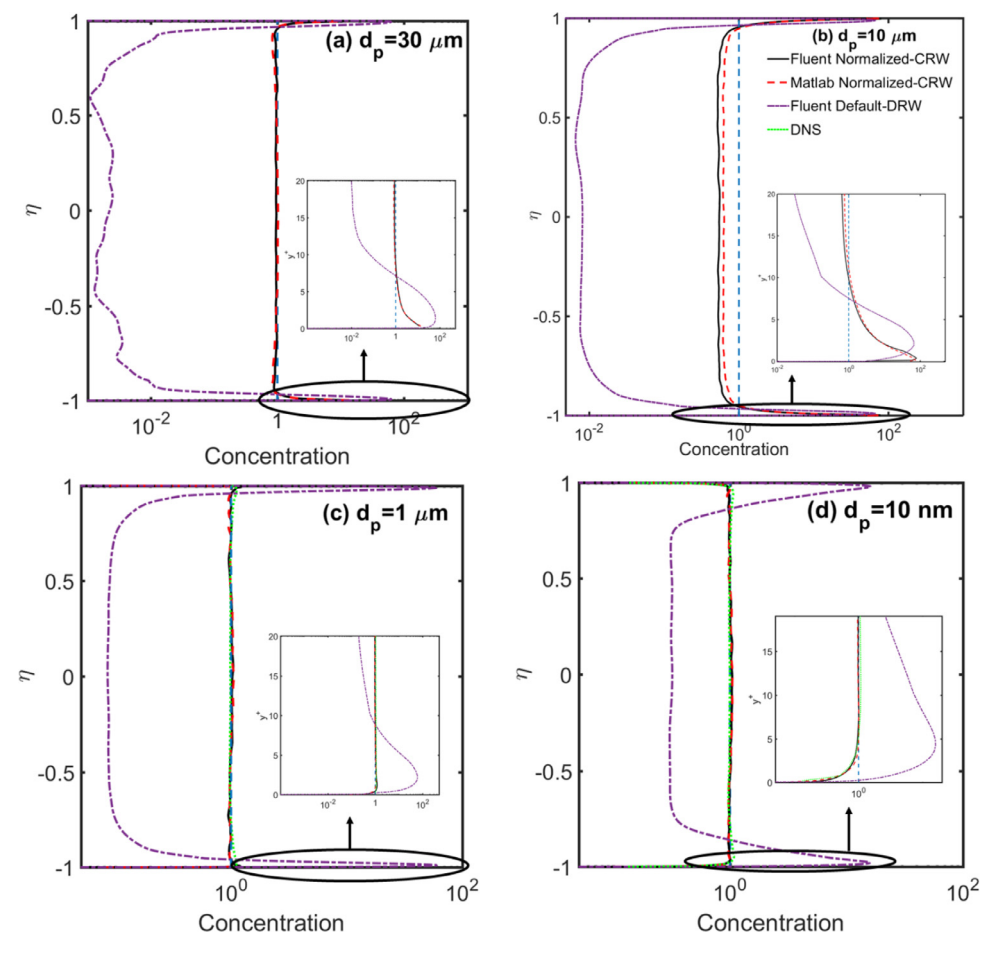


Fig. 13. Comparison of the predictions of different models of the normalized concentration profile of particles with diameters of (a) 30 μm ($\tau_p^+ = 30.30$), (b) 10 μm ($\tau_p^+ = 3.41$), (c) 1 μm ($\tau_p^+ = 3.94 \times 10^{-2}$), and (d) 10 nm ($\tau_p^+ = 1.27 \times 10^{-4}$).

model also allows for the replacement of deposited particles by new particles into the channel through which the total concentration of particles is kept constant. All simulations conducted by the default stochastic turbulence model of the software were repeated using the Normalized-CRW model. As expected, the simulation results obtained by the ANSYS-Fluent software augmented with the Normalized-CRW model were almost identical to those of the Matlab Normalized-CRW model presented in Section 3.3. Therefore, the predictions of the Fluent Normalized-CRW model are not presented here for brevity. However, comparisons of the concentrations, particle velocities, and deposition velocities of different size particles predicted by the Fluent Normalized-CRW model with those of Fluent Default-DRW and Matlab Normalized-CRW are presented in the next section.

3.5. Comparison

In this section, the results obtained from the Fluent Default-DRW model, the in-house Matlab Normalized-CRW, and ANSYS-Fluent Normalized-CRW models are compared, and the advantages of the Normalized-CRW model over the Default-DRW model of the commercial software are discussed. In addition, the agreement of the prediction of the in-house Matlab's code and the Fluent Normalized-CRW is highlighted.

Fig. 13 compares the concentration profiles as predicted by the Fluent Default-DRW model, the in-house Matlab Normalized-CRW model, and the ANSYS-Fluent code with the Normalized-CRW UDF for $30\,\mu m$, $10\,\mu m$, $1\,\mu m$, and $10\,n m$ particles. The concentration profiles for $1\,\mu m$ and $10\,n m$ particles, as obtained from the DNS are

also plotted in this figure to verify the homogenous concentration profiles predicted by the Normalized-CRW model for submicron particles. Since the concentration predicted by the Default-DRW varies with time, in this figure, the profile at t=10,000 wall units was used for comparison. Since the concentration profiles in the near-wall region are very important, the magnified model predictions in this region are also plotted in this figure.

Fig. 13 shows good agreements of the steady state concentration profiles obtained by the in-house Matlab Normalized-CRW model, the ANSYS-Fluent with the Normalized-CRW model, and the DNS results, while clearly illustrating the huge discrepancies of the Fluent Default-DRW model. The Default-DRW model seems to lead to an overactive turbophoresis effect and to the continuous over-migration of particles from the core of the channel toward the near-wall regions, resulting in the unsteady concentration profiles found for all particle sizes, as well as, unrealistically high levels of accumulation of fine particles in the near-wall region.

Another issue is that the default trap boundary condition used in the ANSYS-Fluent code assumes that particles are deposited when their centers reach the wall (instead of reaching d/2). This leads to unphysical results, which is more clearly seen for large particles. Fig. 13a shows that the default model predicts the presence of 30 μ m particles in the region with wall-distance less than the radius of these particles. This is in contrast to the predictions of Matlab Normalized-CRW and Fluent Normalized-CRW simulations that use the correct boundary condition leading to no 30 μ m particles within a distance of 15 μ m from the wall.

The prediction of different models for the mean velocities and RMS velocity fluctuations of 30 µm particles are shown in Fig. 14.

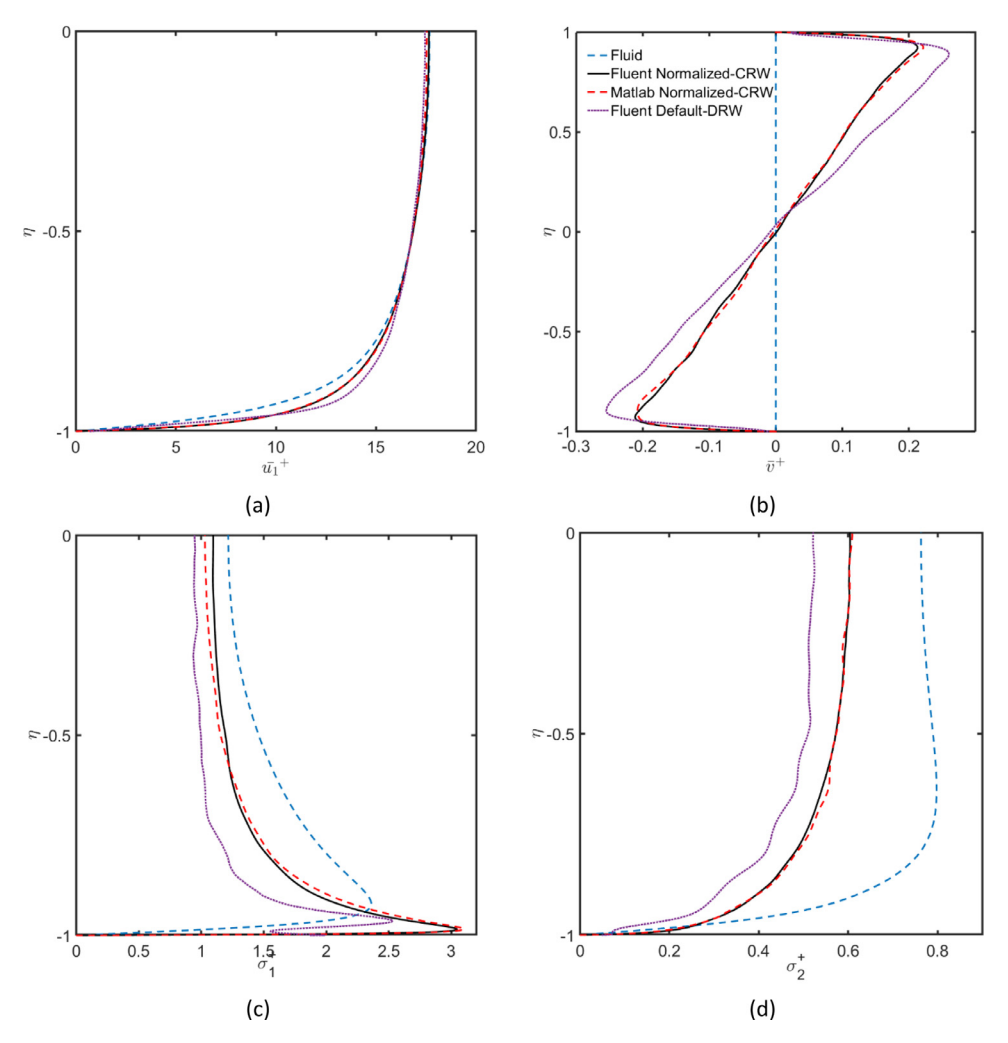


Fig. 14. Comparison of the predictions of different models of the (a) mean streamwise velocity, (b) mean normal velocity, (c) RMS streamwise velocity fluctuations, and (d) RMS normal velocity fluctuations of particles with a diameter of 30 μm.

Again, these figures confirm the consistency between the results obtained by the in-house Matlab CRW model and the ANSYS-Fluent with the Normalized-CRW model, while the ANSYS-Fluent Default-DRW models show significant discrepancies.

In Fig. 15a, the normalized number of deposited particles of different sizes, as estimated by different models, is plotted. This figure shows the good agreement of the predictions of the in-house Matlab Normalized-CRW model and the ANSYS-Fluent with the Normalized-CRW model. However, the number of deposited particles predicted by the Default-DRW model for 30 µm and 10 µm reduce with time, and after the 4000 wall units, almost no particle deposit. The prediction of the DRW model for 100 nm roughly matches the predictions of the Normalized-CRW model, but after around 5000 wall units, it deviates to larger values. The DRW predictions for 100, 50, and 10 nm roughly match those of the Normalized-CRW model at the beginning of the simulation, but after the accumulation of particles in the near-wall regions, they deviate to larger values. In Fig. 15b, the predicted deposition velocities versus time are shown using the number of deposited particles in Eq. (25). As expected, the deposition velocity predicted by the Normalized-CRW models for every size reaches a roughly steady value, while the predicted deposition velocity of the DRW model varies with time and decrease or increase, respectively, for large size and submicron particles. As it was noted in the discussion of Fig. 8, both the decrease and increase of the deposition velocities for large size and submicron particles are due to the spurious accumulation of particles in the near-wall regions generated by the DRW simulations.

In Fig. 16, the RMS particle streamwise and normal velocity fluctuations, as well as the concentration profiles near the lower wall of the channel as predicted by the Default-DRW model, are compared with those evaluated with the use of the Normalized-CRW model. Fig. 16a clearly illustrates the smaller magnitude of the particles RMS streamwise velocity fluctuations predicted by the DRW model in comparison to those of the Normalized-CRW model. In Fig. 16b, the RMS normal velocity fluctuation profiles are plotted. As it was noted in the discussion of Fig. 3, for the simulations of the Default-DRW model, the values of σ_2^+ as computed by the ANSYS-Fluent code without additional correction was used, but for the code with the Normalized-CRW model, σ_2^+ was modified by Eq. (5) in the near-wall region. Hence, the RMS normal particle velocity fluctuations resulting from the Default-DRW model should be compared with fluid default σ_2^+ , while those of the Normalized-CRW model should be compared with the modified σ_2^+ . Fig. 16b shows that the Default-DRW model generates smaller fluctuations for particles in the near-wall region than that of the fluid and Normalized-CRW model. The predictions of the Normalized-CRW model for particle fluctuations are in good agreement with the corrected σ_2^+ of the fluid.

The concentration profiles shown in Fig. 16b reveal interesting details regarding the defects of the Default-DRW model. As it is seen, the Default-DRW model predicts an unrealistically high

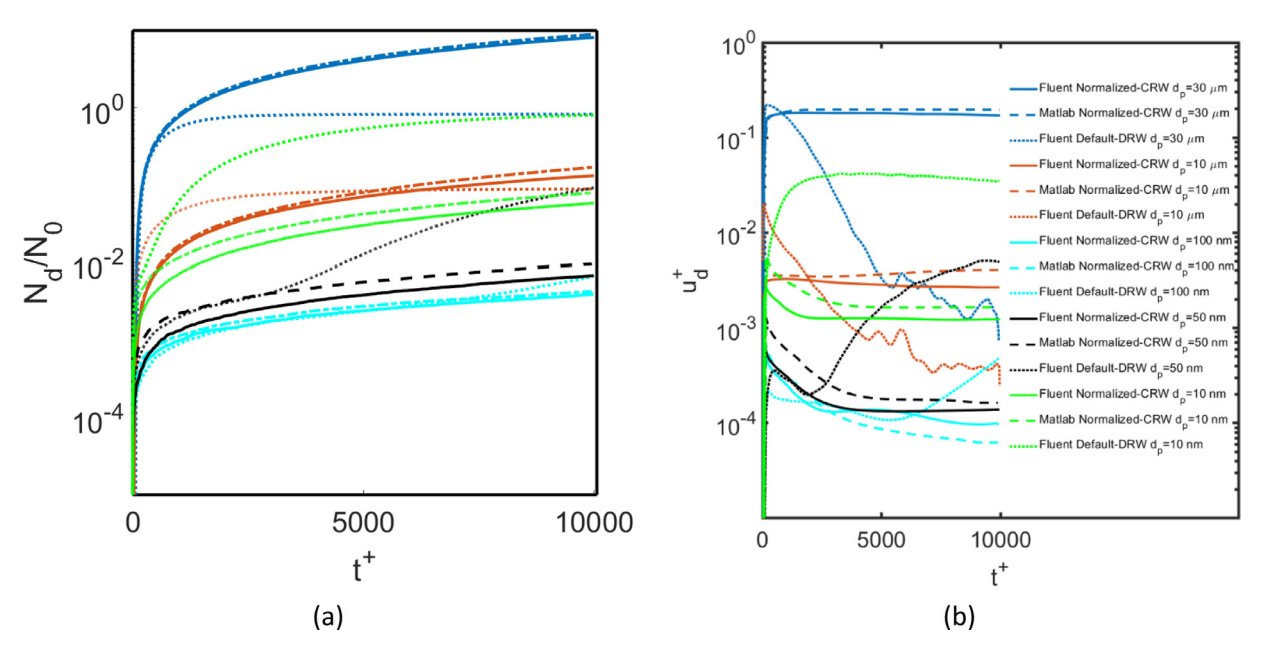


Fig. 15. Comparison of the different model predictions of (a) the normalized number of deposited $30\,\mu m$ to $10\,n m$ particles in time and (b) the non-dimensional predicted deposition velocities.

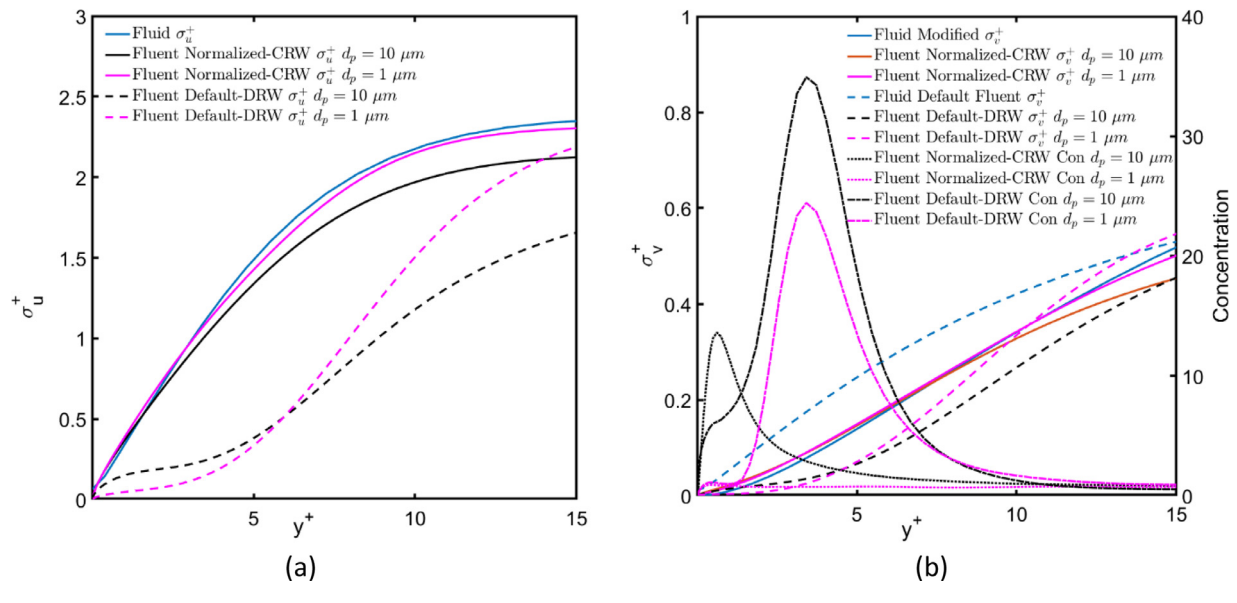


Fig. 16. Comparison the (a) RMS streamwise velocity fluctuations, (b) RMS normal velocity fluctuations, and concentration profiles of particles with diameters of 10 μm and 1 μm near the lower wall of the channel as predicted by the ANSYS-Fluent using the Default-DRW model and the Normalized-CRW model.

concentration in the near-wall regions for all particle sizes. In addition, the location of the concentration peaks predicted by the DRW model for 10 µm particles is at about 5 wall units away from the wall, while the smaller peak predicted by the Normalized-CRW model is much closer to the wall at about 1 wall unit. The high concentration of 10 µm in the near-wall region is due to the turbophoresis effects as a result of the gradient of the fluid RMS normal velocity fluctuations. The DNS results of Marchioli et al. (2007) show that the peak concentration of inertial particles occurs at $y^+ \le 1$, which is in agreement with the predictions of the Normalized-CRW model. The Default-DRW model, however, predicts the location of the peak concentration of 10 µm farther away at the edge of the viscous sublayer at $y^+=5$. It is conjectured that the damping of RMS velocity fluctuations near the wall increases the gradient of the normal RMS velocity fluctuations in the near-wall region that results in increasing the tur-

bophoresis effects and shifting the location of peak accumulation of particles. In addition, since the drift correction term is missed in the Default-DRW model, the accumulation of particles in the nearwall regions is predicted for all particle sizes, including the submicrometer particles. The overdamping of the RMS normal velocity fluctuations also leads to trapping of large size particles in this region since they do not maintain sufficient normal velocity fluctuations to escape from the near-wall region or get deposited on the walls. Therefore, the number of particles trapped in the near-wall region continuously increases. For submicron particles, the Default-DRW model still leads to continuous accumulation of particles in the near-wall regions, but they get deposited on the wall because of their large Brownian motions.

In Fig. 17, the dimensionless deposition velocities of different size particles predicted by the Default-DRW, Matlab Normalized-CRW, and Fluent Normalized-CRW models are plotted versus the

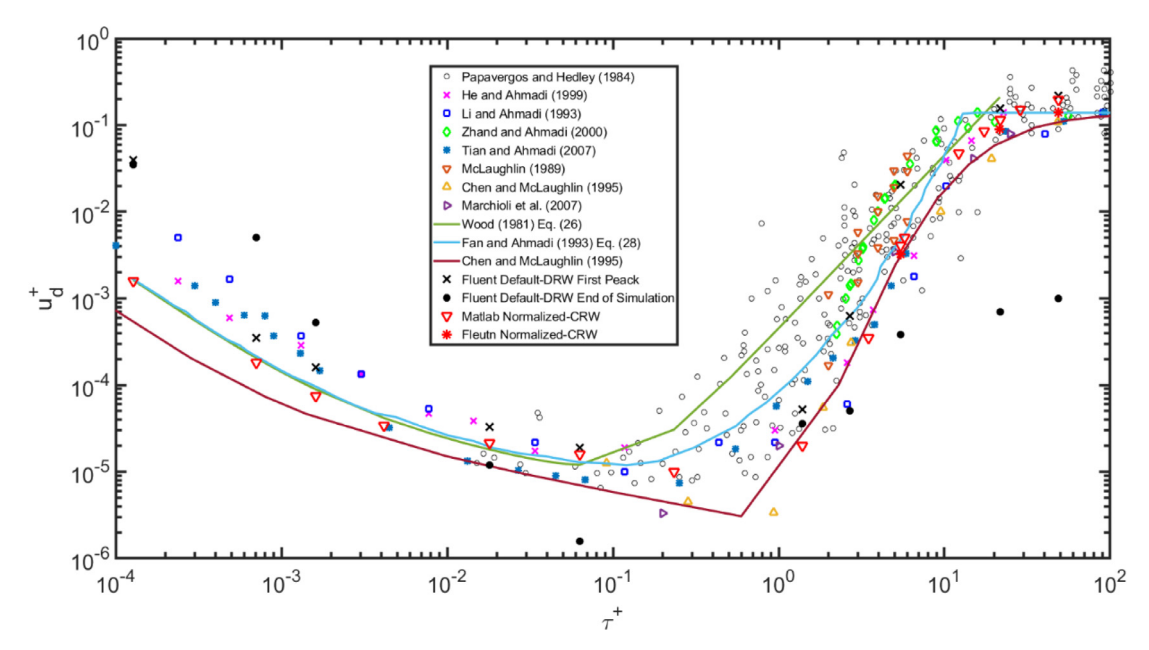


Fig. 17. Comparison of the predicted deposition velocity of various size particles using different stochastic models with the experimental data and empirical models.

corresponding particle relaxation time in wall units. The experimental data of deposition velocity collected by Papavergos and Hedley (1984), the earlier numerical results (Li and Ahmadi 1993; He and Ahmadi 1999; Tian and Ahmadi 2007), the DNS results (McLaughlin 1989; Chen and McLaughlin 1995; Zhang and Ahmadi 2000; Marchioli et al., 2007), and those obtained from empirical equations for channel flows (Wood 1981; Fan and Ahmadi 1993) are also shown in this figure for comparison. In addition, the estimations of deposition velocity predicted by Guingo and Minier (2008) and Jin et al. (2015) that statistically included the effects of near-wall coherent structures are also plotted in this figure. While using these models requires more effort, they predict reasonable deposition velocities. For the Matlab Normalized-CRW and Fluent Normalized-CRW, the steady state deposition velocity predicted by the models is plotted in Fig. 17. However, since it is not possible to get a steady state deposition velocity for the Default-DRW model, the deposition velocity predicted at the beginning (first peak) and the end of simulation (after 10,000 wall units) are shown in Fig. 17 and labeled as "Fluent Default-DRW First Peak" and "Fluent Default-DRW End of Simulation." This figure shows that the deposition velocities predicted by the Fluent Normalized-CRW and Matlab Normalized-CRW match each other, and they are in good agreement with the experimental data for inertial particles, the DNS and with the empirical model predictions including the Brownian particles. The agreement of the current deposition velocity predictions, especially for Brownian particles, with the available data is more accurate than the deposition velocities reported by Javaraju et al. (2015).

Fig. 17, however, shows that the deposition velocity predicted by the Default-DRW model (end of simulation) overpredicts the deposition velocity for particles smaller than 500 nm and underpredicts the data for larger particles. As noted in the discussion of Fig. 8, the predicted deposition velocity for particles with d < 500 nm increases with time of simulation, and for large particles, the deposition velocity decreases in time. Thus, these lead to incorrect predictions of the DRW models for long-duration simulations. The predictions of the Default-DRW model using the first peak deposition rate values in the early part of simulations are also compared with the experimental data and numerical results in Fig. 17. It is seen that the model prediction for the deposition velocity is in reasonable agreement with the data. It should

be pointed out that early in the simulations the concentration of particles is roughly uniform and the DRW model predictions for the deposition velocity is not far off, but as particles accumulate in the near-wall regions $2 < y^+ < 8$, the corresponding prediction for the deposition velocity loses its accuracy.

4. Conclusions

The mean flow velocities and RMS velocity fluctuations of a turbulent flow in a channel were evaluated using the RANS-RSTM turbulence model of the ANSYS-Fluent 18.1 code. Then, the trajectories of nano- and micro-particles were evaluated using the DPM of the ANSYS-Fluent code, as well as an in-house Matlab particle tracking code. To include the effect of instantaneous fluid velocity fluctuations on particle dispersion, the Default-DRW stochastic model of the ANSYS-Fluent code and the Normalized-CRW stochastic model were used in the simulations. The concentration profiles and deposition velocities of different size particles as predicted by the ANSYS-Fluent and the Matlab simulations were compared with the available experimental data, earlier simulation results, and empirical equations. The accuracy of the Default-DRW and Normalized-CRW stochastic models in generating the fluid velocity fluctuations in inhomogeneous turbulent flows for submicron and inertial particles was carefully examined. Based on the presented results, the following conclusions are drawn:

- The Default-DRW model predicts a continuous migration of the particles toward the walls and fails to lead to steady concentration distributions for different size particles. As a result, the corresponding particle deposition velocities also evolve with time.
- The Default-DRW model appears to underestimate the streamwise and normal particle RMS velocity fluctuations in a band near the wall. Thus, the gradient of the normal RMS velocity fluctuations seen by particles increases unrealistically compared to that of the fluid RMS velocity fluctuations.
- The unphysical increase of the normal RMS velocity fluctuations gradient in the near-wall region and ignoring the drift correction term in the Default-DRW model lead to an overestimation of the turbophoresis effects for inertial particles and also generate spurious migration of submicron particles toward the wall.

- The inaccuracy of the Default-DRW model is not only due to the spurious drift as it was already reported in the literature, but there is also unreasonable damping of the fluid velocity fluctuations in the near-wall region that leads to additional is-
- The Default-DRW model of the commercial software leads to an unrealistic accumulation of particles of all sizes in a band at about 2<y+<8 near the wall. The deposition velocity of inertial particles continuously decreases with time as they are trapped in the near-wall region and do not have sufficient normal velocity fluctuations. The deposition velocity of submicron particles, however, increases in time because of their large Brownian motion as their concentration increases near the wall.
- For long-duration simulations with the Default-DRW model, the predicted deposition velocities of the inertial particles underestimate the experimental data, while those for Brownian particles overestimate the data.
- The deposition velocity predicted by the Default-DRW model at the beginning of the simulation (near their first peak value), when the distribution of particles is roughly uniform, appears to be in reasonable agreement with the experimental data.
- The simulation results by the Matlab Normalized-CRW model show that using the Normalized-CRW leads to a realistic uniform distribution for submicron particles and also reasonable distribution for inertial particles with appropriate turbophoresis effects in the near-wall regions.
- Comparing the deposition velocity predicted by the Matlab Normalized-CRW with the available data verifies the accuracy of Normalized-CRW model for evaluation of the deposition velocity of nano- and micro-particles in inhomogeneous turbulent
- The implementation of the Normalized-CRW model with the use of UDF into the ANSYS-Fluent code also leads to accurate concentration profiles and to deposition velocities for different size particles that are in good agreement with the experimental data, DNS simulations and empirical model similar to the results obtained by the Matlab Normalized-CRW code.
- The use of the Normalized-CRW model instead of the default-DRW model significantly improved the performance of the ANSYS-Fluent code in predicting the concentration distribution and deposition velocity of different sized particles.
- Although the Normalized-CRW model does not meet all the consistency requirements described by Minier et al. (2014), the presented results show that this model predicts the instantaneous velocity fluctuations seen by particles reasonably well and leads to satisfactory predictions of particle dispersion and deposition, as well as particle concentration in inhomogeneous turbulent flows.
- The Simplified Langevin Model (SLM) requires the implementation of certain assumptions for the near-wall region and particle deposition criteria to accurately predict deposition velocities of small-inertia particles (Guingo and Minier 2008; Chibbaro and Minier, 2008). However, the normalized Langevin equation appears to predict the deposition velocity and concentration profiles for a wide range of particle size with reasonable accuracy and is simple to implement in commercial codes.

Note that the inclusion of explicit viscous effects in the Langevin equation that could be important in the near-wall region as discussed by Ahmadi and Hayday (1988), Wacławczyk et al. (2004), and others is still unresolved and is left for future studies.

Declaration of Competing Interest

This is to confirm that the authors do not have a conflict of interest.

References

- Afkhami, M., Hassanpour, A., Fairweather, M., Niobuenwu, D.O., 2015, Particle agglomeration and dispersion in fully-coupled turbulent channel flow using large eddy simulation and discrete element method. Procedia Eng. 102, 780-789.
- Ahmadi, G., Hayday, A., 1988. A probability density closure model for turbulence. Acta Mech. 72 (1-2), 55-71.
- ANSYS: ANSYS fluent theory guide 14.0. ANSYS, Canonsburg, PA (2011).
- ANSYS: ANSYS fluent theory guide 18.0. ANSYS, Canonsburg, PA (2017).
- Antonia, R., Kim, I., Browne, L., 1991, Some characteristics of small-scale turbulence in a turbulent duct flow. I. Fluid Mech. 233, 369-388.
- Bocksell, T., Loth, E., 2006. Stochastic modeling of particle diffusion in a turbulent boundary layer. Int. J. Multiph. Flow 32 (10), 1234-1253.
- Bocksell, T.L., Loth, E., 2001. Random walk models for particle diffusion in free-shear
- flows. AIAA J. 39 (6), 1086–1096. Brooke, J.W., Hanratty, T., McLaughlin, J.: Free-flight mixing and deposition of aerosols. 6(10), 3404-3415 (1994).
- Brooke, J.W., Kontomaris, K., Hanratty, T., McLaughlin, J.B., 1992. Turbulent deposition and trapping of aerosols at a wall. Phys. Fluids A Fluid Dyn. 4 (4), 825-834.
- Caporaloni, M., Tampieri, F., Trombetti, F., Vittori, O., 1975. Transfer of particles in nonisotropic air turbulence. J. Atmosp. Sci. 32 (3), 565-568.
- Chen, M., McLaughlin, J.B., 1995. A new correlation for the aerosol deposition rate in vertical ducts. J. Colloid Interface Sci. 169 (2), 437-455.
- Cheng, Y.S., 2003. Aerosol deposition in the extrathoracic region. Aerosol. Sci. Technol. 37 (8), 659-671.
- Chibbaro, S., Minier, J.-.P., 2008. Langevin PDF simulation of particle deposition in a turbulent pipe flow. J. Aerosol. Sci. 39 (7), 555-571.
- Chibbaro, S., Minier, J.-.P., 2011. A note on the consistency of hybrid Eulerian/Lagrangian approach to multiphase flows. Int. J. Multiph. Flow 37 (3), 293-297
- Colucci, P., Jaberi, F., Givi, P., Pope, S., 1998. Filtered density function for large eddy simulation of turbulent reacting flows. Phys. Fluids 10 (2), 499-515
- Dehbi, A., 2008. Turbulent particle dispersion in arbitrary wall-bounded geometries: a coupled CFD-Langevin-equation based approach. Int. J. Multiph. Flow 34 (9), 819-828.
- Dehbi, A., 2010. Validation against DNS statistics of the normalized Langevin model for particle transport in turbulent channel flows. Powder Technol. 200 (1),
- Devenish, B., Bartello, P., Brenguier, J.L., Collins, L., Grabowski, W., IJzermans, R., Malinowski, S., Reeks, M., Vassilicos, J., Wang, L.P., 2012. Droplet growth in warm turbulent clouds. Q. J. R. Meteorol. Soc. 138 (667), 1401-1429.
- Dreeben, T.D., Pope, S.B., 1997. Probability density function and Reynolds-Stress modeling of near-wall turbulent flows. Phys. Fluids (1994-present) 9 (1), 154-163
- Durbin, P., 1993. A Reynolds stress model for near-wall turbulence. J. Fluid Mech. 249, 465-498.
- Durbin, P.A., 1983. Stochastic Differential Equations and Turbulent Dispersion. NASA Reference Publication, p. 1103.
- Durbin, P.A., 1984. Comments on papers by Wilson et al.(1981) and Legg and Raupach (1982). Boundary Layer Meteorol. 29 (4), 409-411.
- Fan, F.-.G., Ahmadi, G., 2000. Wall deposition of small ellipsoids from turbulent air flows-a Brownian dynamics simulation. J. Aerosol. Sci. 31 (10), 1205-1229.
- Fan, F., Ahmadi, G., 1993. A sublayer model for turbulent deposition of particles in vertical ducts with smooth and rough surfaces. J. Aerosol. Sci. 24 (1), 45-64.
- Finnicum, D.S., Hanratty, T.J., 1985. Turbulent normal velocity fluctuations close to a wall. Phys. Fluids 28 (6), 1654-1658.
- Givi, P., 1989. Model-free simulations of turbulent reactive flows. progress. Energy Combust. Sci. 15 (1), 1-107.
- Gosman, A., Ioannides, E., 1983. Aspects of computer simulation of liquid-fueled combustors. J. Energy 7 (6), 482-490.
- Guingo, M., Minier, J.-.P., 2008. A stochastic model of coherent structures for particle deposition in turbulent flows. Phys. Fluids 20 (5), 053303.
- Hall, C., 1975. The simulation of particle motion in the atmosphere by a numerical random-walk model. Q. J. R. Meteorol. Soc. 101 (428), 235-244.
- Hanjalić, K., Launder, B., 1972. A Reynolds stress model of turbulence and its application to thin shear flows. J Fluid Mech 52 (4), 609-638.
- Haworth, D., Pope, S., 1986. A generalized Langevin model for turbulent flows. Phys. Fluids 29 (2), 387-405.
- Haworth, D., Pope, S., 1987. A pdf modeling study of self-similar turbulent free shear flows. Phys. Fluids 30 (4), 1026-1044.
- He, C., Ahmadi, G., 1999. Particle deposition in a nearly developed turbulent duct flow with electrophoresis. J. Aerosol. Sci. 30 (6), 739-758.
- Hinds, W.C., 1982. Aerosol Technology: Properties, Behavior, and Measurement of Airborne Particles. John Wiley & Sons.
- Hinze, J., 1975. Turbulence, 218. McGraw-Hill, New York.
- Iliopoulos, I., Hanratty, T.J., 1999. Turbulent dispersion in a non-homogeneous field. J. Fluid Mech. 392, 45-71.
- Iliopoulos, I., Mito, Y., Hanratty, T.J., 2003. A stochastic model for solid particle dispersion in a nonhomogeneous turbulent field. Int. I. Multiph. Flow 29 (3). 375-394.
- Innocenti, A., Marchioli, C., Chibbaro, S., 2016. Lagrangian filtered density function for LES-based stochastic modelling of turbulent particle-laden flows. Phys. Fluids 28 (11), 115106.
- Jayaraju, S., Brouns, M., Lacor, C., Belkassem, B., Verbanck, S., 2008. Large eddy and detached eddy simulations of fluid flow and particle deposition in a human mouth-throat, I. Aerosol, Sci. 39 (10), 862-875.

- Jayaraju, S., Sathiah, P., Roelofs, F., Dehbi, A., 2015. RANS modeling for particle transport and deposition in turbulent duct flows: near wall model uncertainties. Nucl. Eng. Des. 289, 60–72.
- Jin, C., Potts, I., Reeks, M., 2015. A simple stochastic quadrant model for the transport and deposition of particles in turbulent boundary layers. Phys. Fluids 27 (5), 053305.
- Jin, C., Potts, I., Reeks, M., 2016. The effects of near wall corrections to hydrodynamic forces on particle deposition and transport in vertical turbulent boundary layers. Int. J. Multiph. Flow 79, 62–73.
- Kaftori, D., Hetsroni, G., Banerjee, S., 1995. Particle behavior in the turbulent boundary layer. II. Velocity and distribution profiles. Phys. Fluids 7 (5), 1107–1121.
- Kallio, G., Reeks, M., 1989. A numerical simulation of particle deposition in turbulent boundary layers. Int. J. Multiph. Flow 15 (3), 433–446.
- Kim, J., Moin, P., Moser, R., 1987. Turbulence statistics in fully developed channel flow at low Reynolds number. J. Fluid Mech. 177, 133–166.
- edited by Kuerten, J., 2005. A subgrid model for large-eddy simulation of particle-laden channel flow. In: Sommerfeld, M. (Ed.), Proceedings of the 11th Workshop on Two-Phase Flow Predictions edited by.

 Kuerten, J., Vreman, A., 2005. Can turbophoresis be predicted by large-eddy simu-
- Kuerten, J., Vreman, A., 2005. Can turbophoresis be predicted by large-eddy simu lation? Phys. Fluids 17 (1), 011701-011701.
- Legg, B., 1982. Turbulent dispersion from an elevated line source: Markov chain simulations of concentration and flux profiles. Q. J. R. Meteorol. Soc. 109 (461), 645–660.
- Legg, B., Raupach, M., 1982. Markov-chain simulation of particle dispersion in inhomogeneous flows: the mean drift velocity induced by a gradient in Eulerian velocity variance. Bound. Layer Meteorol. 24 (1), 3–13.
- Lesieur, M., Métais, O., Comte, P., 2005. Large-Eddy Simulations of Turbulence. Cambridge university press.
- Ley, A.J., Thomson, D., 1983. A random walk model of dispersion in the diabatic surface layer. Q. J. R. Meteorol. Soc. 109 (462), 867–880.
- Li, A., Ahmadi, G., 1992. Dispersion and deposition of spherical particles from point sources in a turbulent channel flow. Aerosol. Sci. Technol. 16 (4), 209–226.
- Li, A., Ahmadi, G., 1993. Deposition of aerosols on surfaces in a turbulent channel flow. Int. J. Eng. Sci. 31 (3), 435–451.
- Longest, P.W., Hindle, M., Choudhuri, S.D., Xi, J., 2008. Comparison of ambient and spray aerosol deposit in a standard induction port and more realistic
- mouth-throat geometry. J. Aerosol. Sci. 39 (7), 572–591.
 Longest, P.W., Vinchurkar, S., 2009. Inertial deposition of aerosols in bifurcating
- models during steady expiratory flow. J. Aerosol. Sci. 40 (4), 370–378. Loth, E., 2000. Numerical approaches for motion of dispersed particles, droplets and
- bubbles. Progress Energy Combust. Sci. 26 (3), 161–223. Luo, K., Yu, H., Dai, Z., Fang, M., Fan, J., 2016. CFD simulations of flow and dust dispersion in a realistic urban area. Eng. Appl. Comput. Fluid Mech. 10 (1),
- 228–242.

 MacInnes, J., Bracco, F., 1992. Stochastic particle dispersion modeling and the trac-
- er-particle limit. Phys. Fluids A Fluid Dyn. 4 (12), 2809–2824. Mansour, N.N., Kim, J., Moin, P., 1988. Reynolds-stress and dissipation-rate budgets
- in a turbulent channel flow. J. Fluid Mech. 194, 15–44.
 Marchioli, C., 2017. Large-eddy simulation of turbulent dispersed flows: a review of
- modelling approaches. Acta Mech. 228 (3), 741–771.

 Marchioli, C., Picciotto, M., Soldati, A., 2007. Influence of gravity and lift on particle velocity statistics and transfer rates in turbulent vertical channel flow. Int. J.
- Multiph. Flow 33 (3), 227–251.

 Marchioli, C., Salvetti, M., Soldati, A., 2008. Some issues concerning large-eddy simulation of inertial particle dispersion in turbulent bounded flows. Phys. Fluids 20 (4), 040603.
- Marchioli, C., Soldati, A., 2002. Mechanisms for particle transfer and segregation in a turbulent boundary layer. J. Fluid Mech. 468, 283–315.
- Matida, E., Finlay, W., Lange, C., Grgic, B., 2004. Improved numerical simulation of aerosol deposition in an idealized mouth-throat. J. Aerosol. Sci. 35 (1), 1–19.
- Matida, E.A., Nishino, K., Torii, K., 2000. Statistical simulation of particle deposition on the wall from turbulent dispersed pipe flow. Int. J. Heat Fluid Flow 21 (4), 389–402
- McLaughlin, J.B., 1989. Aerosol particle deposition in numerically simulated channel flow. Phys. Fluids A Fluid Dyn. (1989-1993) 1 (7), 1211–1224.
- Minier, J.-.P., 2015. On Lagrangian stochastic methods for turbulent polydisperse two-phase reactive flows. Prog. Energy Combust. Sci. 50, 1-62.
- Minier, J.-P., Chibbaro, S., Pope, S.B., 2014. Guidelines for the formulation of Lagrangian stochastic models for particle simulations of single-phase and dispersed two-phase turbulent flows. Phys. Fluids 26 (11), 113303.
- Minier, J.-.P., Peirano, E., 2001. The pdf approach to turbulent polydispersed two-phase flows. Phys. Rep. 352 (1), 1–214.
- Minier, J.-.P., Peirano, E., Chibbaro, S., 2004. PDF model based on Langevin equation for polydispersed two-phase flows applied to a bluff-body gas-solid flow. Phys. Fluids 16 (7), 2419–2431.
- Mofakham, A.A., Ahmadi, G., 2019. Particles dispersion and deposition in inhomogeneous turbulent flows using continuous random walk models. Phys. Fluids 31 (8), 13.
- Mofakham, A.A., Ahmadi, G., McLaughlin, J., 2018. Interactions of flow structure with Nano-and micro-particles in turbulent channel flows. In: Proceedings of the ASME 2018 5th Joint US-European Fluids Engineering Division Summer Meeting V003T019A003American Society of Mechanical Engineers.
- Morsi, S., Alexander, A., 1972. An investigation of particle trajectories in two-phase flow systems. J. Fluid Mech. 55 (02), 193–208.
- Moser, R.D., Kim, J., Mansour, N.N., 1999. Direct numerical simulation of turbulent channel flow up to re τ = 590. Phys. Fluids 11 (4), 943–945.

- Narayanan, C., Lakehal, D., Botto, L., Soldati, A., 2003. Mechanisms of particle deposition in a fully developed turbulent open channel flow. Phys. Fluids 15 (3), 763–775.
- Nasr, H., Ahmadi, G., McLaughlin, J.B., 2009. A DNS study of effects of particle-particle collisions and two-way coupling on particle deposition and phasic fluctuations. J. Fluid Mech. 640, 507-536.
- Ounis, H., Ahmadi, G., McLaughlin, J.B., 1991. Brownian diffusion of submicrometer particles in the viscous sublayer. J. Colloid Interface Sci. 143 (1), 266–277.
- Ounis, H., Ahmadi, G., McLaughlin, J.B., 1993. Brownian particle deposition in a directly simulated turbulent channel flow. Phys. Fluids A Fluid Dyn. 5 (6), 1427–1432.
- Papavergos, P., Hedley, A., 1984. Particle deposition behaviour from turbulent flows. Chem. Eng. Res. Des. 62 (5), 275–295.
- Pope, S.B., 1985. PDF methods for turbulent reactive flows. Prog. Energy Combust. Sci. 11 (2), 119–192.
- Pope, S.B., 2000. Turbulent Flows. Cambridge University Press, Cambridge.
- Pozorski, J., 2017. Models of turbulent flows and particle dynamics. In: Particles in Wall-Bounded Turbulent Flows: Deposition, Re-Suspension and Agglomeration. Springer, pp. 97–150.
- Rahman, M., Cheng, W., Samtaney, R., Urzay, J., 2016. Large-eddy simulations of sandstorms as charged-particle suspensions in turbulent boundary layers. In: Proceedings of the Summer Program, p. 45.
- Rashidi, M., Hetsroni, G., Banerjee, S., 1990. Particle-turbulence interaction in a boundary layer. Int. J. Multiph. Flow 16 (6), 935–949.
- Reeks, M., 1981. The transport of discrete particles in turbulent shear flow. In: Proceedings of the Conference on Gas-Borne Particles. Institutte of Mechanical Engineering., Oxford, England, pp. 87–92.
- Reeks, M., 1983. The transport of discrete particles in inhomogeneous turbulence. J. Aerosol. Sci. 14 (6), 729–739.
- Reid, J.D., 1979. Markov chain simulations of vertical dispersion in the neutral surface layer for surface and elevated releases. Bound. Layer Meteorol. 16 (1), 3–22.
- Rogallo, R.S., Moin, P., 1984. Numerical simulation of turbulent flows. Annu. Rev. Fluid Mech. 16 (1), 99–137.
- Sagaut, P., 2006. Large Eddy Simulation for Incompressible flows: an Introduction. Springer Science & Business Media.
- Sajjadi, H., Tavakoli, B., Ahmadi, G., Dhaniyala, S., Harner, T., Holsen, T., 2016. Computational fluid dynamics (CFD) simulation of a newly designed passive particle sampler. Environ. Pollut. 214, 410–418.
- Salmanzadeh, M., Rahnama, M., Ahmadi, G., 2010. Effect of sub-grid scales on large eddy simulation of particle deposition in a turbulent channel flow. Aerosol. Sci. Technol. 44 (9), 796–806.
- Shi, H., Kleinstreuer, C., Zhang, Z., 2008. Dilute suspension flow with nanoparticle deposition in a representative nasal airway model. Phys. Fluids 20 (1), 013301.
- Shirolkar, J., Coimbra, C., McQuay, M.Q., 1996. Fundamental aspects of modeling turbulent particle dispersion in dilute flows. Prog. Energy Combust. Sci. 22 (4), 363–399.
- Tavakol, M., Abouali, O., Yaghoubi, M., Ahmadi, G., 2015. Stochastic dispersion of ellipsoidal fibers in various turbulent fields. J. Aerosol. Sci. 80, 27–44.
- Tavakol, M., Ghahramani, E., Abouali, O., Yaghoubi, M., Ahmadi, G., 2017. Deposition fraction of ellipsoidal fibers in a model of human nasal cavity for laminar and turbulent flows. J Aerosol Sci 113, 52–70.
- Tavakoli, B., Abouali, O., Bagheri, M., Yazdi, M., Ahmadi, G., 2012. Micro particles transport and deposition in realistic geometry of human upper airways. IJE Trans. A Basics 25 (4), 315–322.
- Taylor, G.I., 1920. Diffusion by continuous movements. Proc. Lond. Math. Soc. 2 (1), 196–212.
- Thomson, D., 1984. Random walk modelling of diffusion in inhomogeneous turbulence. Q. J. R. Meteorol. Soc. 110 (466), 1107–1120.
- Tian, L., Ahmadi, G., 2007. Particle deposition in turbulent duct flows—comparisons of different model predictions. J. Aerosol. Sci. 38 (4), 377–397.
- Tian, L., Ahmadi, G., 2012. Transport and deposition of micro-and nano-particles in human tracheobronchial tree by an asymmetric multi-level bifurcation model. J. Comput. Multiph Flows 4 (2), 159–182.
- Tian, L., Ahmadi, G., 2013. Fiber transport and deposition in human upper tracheobronchial airways. J. Aerosol. Sci. 60, 1–20.
- Uijttewaal, W., Oliemans, R., 1996. Particle dispersion and deposition in direct numerical and large eddy simulations of vertical pipe flows. Phys. Fluids 8 (10), 2590–2604.
- van Haarlem, B., Boersma, B.J., Nieuwstadt, F.T., 1998. Direct numerical simulation of particle deposition onto a free-slip and no-slip surface. Phys. Fluids 10 (10), 2608–2620.
- Wacławczyk, M., Pozorski, J., Minier, J.-.P., 2004. Probability density function computation of turbulent flows with a new near-wall model. Phys. Fluids 16 (5), 1410–1422.
- Wacławczyk, M., Pozorski, J., Minier, J.-.P., 2008. New molecular transport model for FDF/LES of turbulence with passive scalar. Flow Turbul. Combust. 81 (1-2), 235.
- Wang, Q., Squires, K., 1996. Large eddy simulation of particle deposition in a vertical turbulent channel flow. Int. J. Multiph. Flow 22 (4), 667–683.
- Warhaft, Z., 2008. Laboratory studies of droplets in turbulence: towards understanding the formation of clouds. Fluid Dyn. Res. 41 (1), 011201.
- Wilson, J., Thurtell, G., Kidd, G., 1981a. Numerical simulation of particle trajectories in inhomogeneous turbulence, II: systems with variable turbulent velocity scale. Bound. Layer Meteorol. 21 (4), 443–463.
- Wilson, J., Thurtell, G., Kidd, G., 1981b. Numerical simulation of particle trajectories in inhomogeneous turbulence, III: comparison of predictions with experimental data for the atmospheric surface layer. Bound. Layer Meteorol. 21 (4), 423–441.

- Wood, N., 1981. A simple method for the calculation of turbulent deposition to smooth and rough surfaces. J. Aerosol. Sci. 12 (3), 275–290. Yazdani, A., Normandie, M., Yousefi, M., Saidi, M., Ahmadi, G., 2014. Transport and
- Yazdani, A., Normandie, M., Yousen, M., Saidi, M., Anmadi, G., 2014. Transport and deposition of pharmaceutical particles in three commercial spacer–MDI combinations. Comput. Biol. Med. 54, 145–155.
 Yeh, F., Lei, U., 1991. On the motion of small particles in a homogeneous isotropic turbulent flow. Phys. Fluids A Fluid Dyn. 3 (11), 2571–2586.

- Young, J., Leeming, A., 1997. A theory of particle deposition in turbulent pipe flow. J. Fluid Mech. 340, 129–159.
 Zamankhan, P., Ahmadi, G., Wang, Z., Hopke, P.K., Cheng, Y.-.S., Su, W.C., Leonard, D., 2006. Airflow and deposition of nano-particles in a human nasal cavity. Aerosol. Sci. Technol. 40 (6), 463–476.
 Zhang, H., Ahmadi, G., 2000. Aerosol particle transport and deposition in vertical and horizontal turbulent duct flows. J. Fluid Mech. 406, 55–80.